JOURNAL OF PETROLOGY | VOLUME 44 | NUMBER 7 | PAGES 1247–1280 | 2003

Quantification of Magmatic and Hydrothermal Processes in a Peralkaline Syenite–Alkali Granite Complex Based on Textures, Phase Equilibria, and Stable and Radiogenic Isotopes

MICHAEL MARKS[1], TORSTEN VENNEMANN[2], WOLFGANG SIEBEL[1] AND GREGOR MARKL[1]*

[1]INSTITUT FÜR GEOWISSENSCHAFTEN, AB MINERALOGIE UND GEODYNAMIK, EBERHARD-KARLS-UNIVERSITÄT, WILHELMSTRASSE 56, D-72074 TÜBINGEN, GERMANY

[2]INSTITUT DE MINÉRALOGIE ET GÉOCHIMIE, UNIVERSITÉ DE LAUSANNE, UNIL–BFSH2, CH-1015 LAUSANNE, SWITZERLAND

RECEIVED AUGUST 28, 2002; ACCEPTED FEBRUARY 19, 2003

The Puklen complex of the Mid-Proterozoic Gardar Province, South Greenland, consists of various silica-saturated to quartz-bearing syenites, which are intruded by a peralkaline granite. The primary mafic minerals in the syenites are augite ± olivine + Fe–Ti oxide + amphibole. Ternary feldspar thermometry and phase equilibria among mafic silicates yield $T = 950–750°C$, $a_{SiO_2} = 0{\cdot}7–1$ *and an* f_{O_2} *of 1–3 log units below the fayalite–magnetite–quartz (FMQ) buffer at 1 kbar. In the granites, the primary mafic minerals are ilmenite and Li-bearing arfvedsonite, which crystallized at temperatures below 750°C and at* f_{O_2} *values around the FMQ buffer. In both rock types, a secondary post-magmatic assemblage overprints the primary magmatic phases. In syenites, primary Ca-bearing minerals are replaced by Na-rich minerals such as aegirine–augite and albite, resulting in the release of Ca. Accordingly, secondary minerals include ferro-actinolite, (calcite–siderite)*$_{ss}$*, titanite and andradite in equilibrium with the Na-rich minerals. Phase equilibria indicate that formation of these minerals took place over a long temperature interval from near-magmatic temperatures down to ~300°C. In the course of this cooling, oxygen fugacity rose in most samples. For example, late-stage aegirine in granites formed at the expense of arfvedsonite at temperatures below 300°C and at an oxygen fugacity above the haematite–magnetite (HM) buffer. The calculated* $\delta^{18}O_{melt}$ *value for the syenites (+5·9 to +6·3‰) implies a mantle origin, whereas the inferred* $\delta^{18}O_{melt}$ *value of* $<+5{\cdot}1‰$ *for the granitic melts is significantly lower. Thus, the granites require an additional low-*$\delta^{18}O$ *contaminant, which was not involved in the genesis of the syenites. Rb/Sr data for minerals of both rock types indicate open-system behaviour for Rb and Sr during post-magmatic metasomatism. Neodymium isotope compositions (*$\varepsilon Nd_{1170\,Ma} = -3{\cdot}8$ *to* $-6{\cdot}4$*) of primary minerals in syenites are highly variable, and suggest that assimilation of crustal rocks occurred to variable extents. Homogeneous* ε_{Nd} *values of −5·9 and −6·0 for magmatic amphibole in the granites lie within the range of the syenites. Because of the very similar neodymium isotopic compositions of magmatic and late- to post-magmatic minerals from the same syenite samples a principally closed-system behaviour during cooling is implied. In contrast, for the granites an externally derived fluid phase is required to explain the extremely low* ε_{Nd} *values of about −10 and low* $\delta^{18}O$ *between +2·0 and +0·5‰ for late-stage aegirine, indicating an open system in the late-stage history. In this study we show that the combination of phase equilibria constraints with stable and radiogenic isotope data on mineral separates can provide much better constraints on magma evolution during emplacement and crystallization than conventional whole-rock studies.*

*Corresponding author. Telephone: +49 (0)7071 2972930. E-mail: markl@uni-tuebingen.de

Journal of Petrology 44(7)

KEY WORDS: *peralkaline; phase equilibria; assimilation; hydrothermal; Li-amphiboles; Greenland; Gardar*

INTRODUCTION

Felsic alkaline igneous rocks can be divided into two principal groups: (1) quartz- and feldspar-bearing, silica-oversaturated rocks; (2) feldspar- and feldspathoid-bearing, silica-undersaturated rocks. The genesis and origin of these two groups is believed to be different. Silica-undersaturated, alkaline, intrusive complexes commonly have isotopic compositions that reflect a magma source in the mantle (e.g. Perry *et al.*, 1987; Kramm & Kogarko, 1994; Dunworth & Bell, 2001). In many cases, contamination or assimilation processes seem to be of minor importance and, consequently, undersaturated alkaline rocks are often interpreted as differentiated residues of benmoreitic or nephelinitic magmas formed in the upper mantle (Larsen & Sørensen, 1987; Kramm & Kogarko, 1994; Stevenson *et al.*, 1997; Frisch & Abdel-Rahman, 1999) under relatively dry conditions and low oxygen fugacities (Harris, 1983; Caroff *et al.*, 1993).

In contrast, based on the close spatial association of silica-undersaturated and silica-oversaturated rocks in many alkaline igneous provinces worldwide, the origin of silica-oversaturated alkaline to peralkaline rocks is often explained by crustal contamination of mantle-derived undersaturated magmas (e.g. Davies & Macdonald, 1987; Foland *et al.*, 1993; Harris, 1995; Mingram *et al.*, 2000; Schmitt *et al.*, 2000; Späth *et al.*, 2001). Studies on alkaline rocks of the midcontinental rift system in North America demonstrated that not only upper crust, but also granulite-facies rocks of the lower crust might interact with alkaline magmas (Heaman & Machado, 1992).

Various experimental studies (e.g. Piotrowski & Edgar, 1970; Sood & Edgar, 1970; Edgar & Parker, 1974; Kogarko & Romanchev, 1977, 1982; Scaillet & Macdonald, 2001) have shown that silica-undersaturated and -oversaturated peralkaline melts have a crystallization interval down to temperatures of ~400°C; the exsolution of a fluid phase from a residual melt is believed to take place in the very late stages of magmatic evolution. There is general consensus that volatiles play a major role in the evolution of alkaline to peralkaline magmas, for both their chemical and physical evolution. Effects of late-stage fluids in some alkaline to peralkaline intrusions of the Gardar Province have been described by Parsons *et al.* (1991), Finch *et al.* (1995), Coulson (1997), Markl (2001), Markl *et al.* (2001) and Markl & Baumgartner (2002). The late-stage fluids expelled from alkaline to peralkaline intrusions are highly enriched in alkalis and incompatible elements. This may result in the formation of aureoles of fenite around alkaline intrusions by interaction with the surrounding country rocks (e.g. Rock, 1976; Kunzendorf *et al.*, 1982; Kresten, 1988; Morogan, 1989) or the autometasomatic formation of secondary mineral assemblages at the expense of primary magmatic minerals within the solidified part of the intrusion itself (e.g. Salvi & Williams-Jones, 1990; Boily & Williams-Jones, 1995; Chakhmouradian & Mitchell, 2002). Recent studies indicate that the sources and isotopic compositions of such a fluid phase may be highly variable (e.g. Boily & Williams-Jones, 1994; Bea *et al.*, 2001) and different isotope systems show variable behaviour with regard to late- or post-magmatic alteration. The resulting isotopic disequilibria between different minerals within a single rock sample may be used to distinguish between primary magmatic and secondary late- to post-magmatic processes.

The Puklen complex of the Gardar Province, South Greenland, is an example of a silica-oversaturated alkaline to peralkaline intrusion comprising a heterogeneous suite of mostly quartz-bearing syenites to quartz-rich peralkaline granite. Petrographically, all rock types show a primary magmatic and a secondary late- to post-magmatic mineral assemblage. The present study is focused on the phase equilibrium constraints on crystallization parameters, on whole-rock geochemistry and on stable and radiogenic isotope compositions of mineral separates, which are used to constrain the magma sources and to decipher the magmatic and late- to post-magmatic processes in the Puklen complex. We show that whole-rock isotope data for these peralkaline rocks would be difficult to interpret and are inadequate for derivation of genetic models.

REGIONAL GEOLOGY

The Gardar Igneous Province (Fig. 1a) in South Greenland represents a failed rift structure of Mid-Proterozoic (1·1–1·3 Ga) age (Upton & Emeleus, 1987). Early Proterozoic (1·7–1·8 Ga) basement granites and gneisses (Emeleus & Upton, 1976) are in places overlain by a sequence of early Gardar basalts and sandstones (Eriksfjord Formation; Poulsen, 1964). A large number of Gardar dyke rocks and about 12 major alkaline to peralkaline igneous complexes intrude the Ketilidian basement. Fluid inclusion data (Poulsen, 1964; Konnerup-Madsen & Rose-Hansen, 1984) and the preserved contacts between sediments and lavas of the Eriksfjord Formation and intrusions indicate that at least the Ilímaussaq intrusion but probably the others as well were intruded at a high crustal level of 3–5 km. The plutonic complexes are composed of (in order of decreasing abundance)

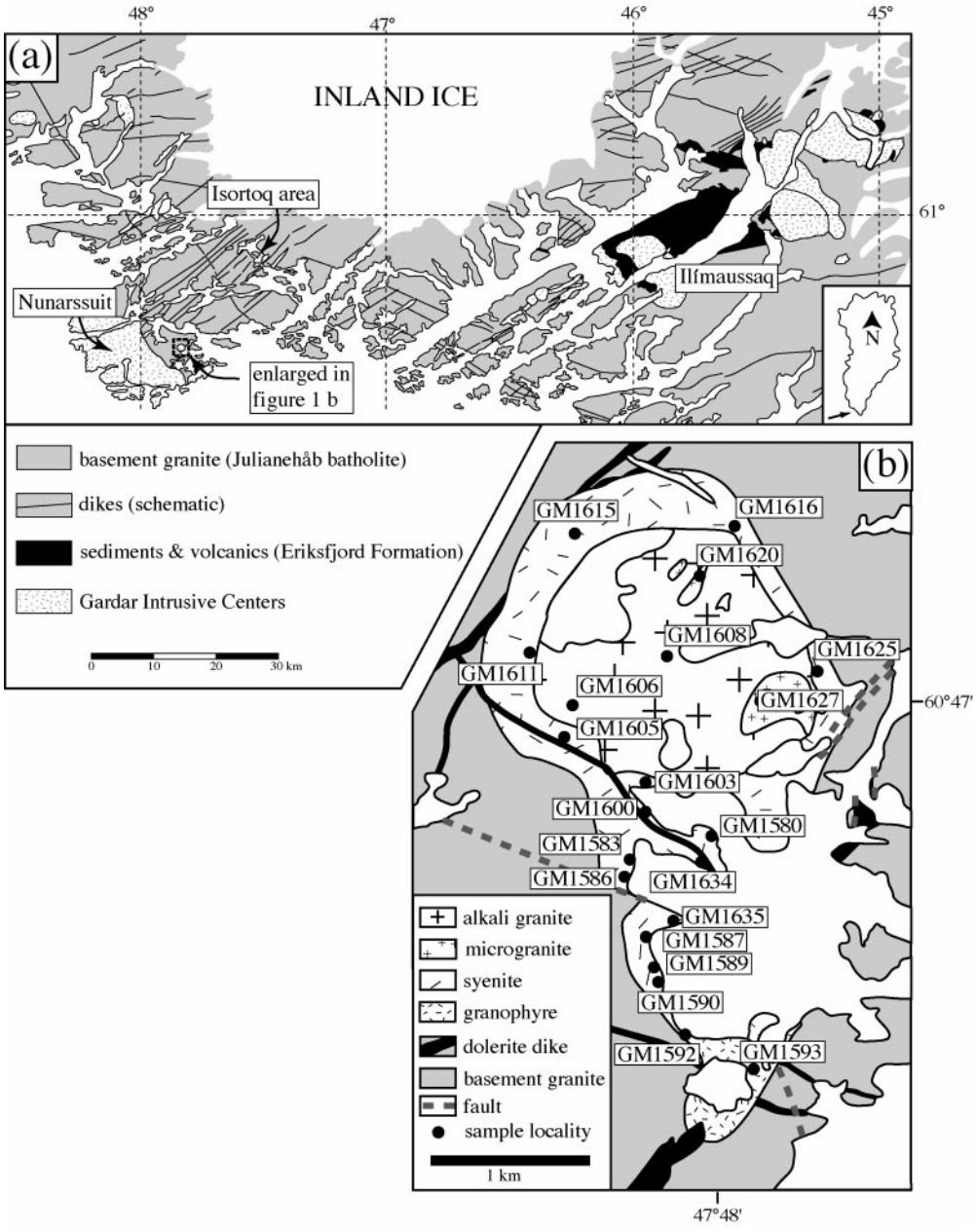

Fig. 1. (a) Sketch map of the alkaline Gardar Province, South Greenland [modified after Escher & Watt (1976)]. The Puklen complex is situated in the western part of the province. Nunarssuit and Ilímaussaq are other alkaline complexes referred to in the text. (b) Enlarged detail of (a). Generalized geological map of the Puklen complex, South Greenland [based on Parsons (1972)]. •, sample localities.

syenites, nepheline syenites, alkali granites, gabbros, syenogabbros and carbonatites. With one exception (the granitic to agpaitic Ilímaussaq intrusion), the major plutonic complexes follow either a SiO_2-undersaturated trend from just saturated syenites to foyaites and peralkaline or agpaitic nepheline syenites, or an oversaturated trend from augite syenites to peralkaline granites. The Puklen complex belongs to the second group.

The Puklen complex (Fig. 1b) is a relatively small body (4 km × 2 km), which intrudes Ketilidian basement granite and early Gardar dolerite dykes. It is cut by NW-trending basic post-Gardar dyke rocks (Pulvertaft, 1961). Hence, the Puklen complex is considered to be of late Gardar age (Pulvertaft, 1961). Zircons from a pegmatite in the nearby Nunarssuit complex have been dated at 1171 ± 5 Ma (Finch *et al.*, 2001). Figure 1b shows a generalized geological

map of the complex. The field geology was described by Parsons (1972). The first magma pulse formed a suite of coarse-grained, fine-grained and porphyritic varieties of silica-saturated to -oversaturated augite syenites. Contacts between the various syenite types are in most cases gradual. Hence, the intrusion of the various syenites probably took place more or less contemporaneously. In the southern part of the intrusion, a fine-grained and leucocratic granophyre cuts the adjoining syenite. A second pulse of magma produced a homogeneous, coarse-grained peralkaline granite, which grades into or may be locally intruded by fine-grained and leucocratic microgranite.

SAMPLES AND ANALYTICAL METHODS

Six syenites, two granophyres, three coarse alkali granites and two microgranites were analysed for their mineral chemical composition, whole-rock chemical compositions and $\delta^{18}O$ values; mineral separates of clinopyroxene and amphibole from selected samples were analysed for O, Sr and Nd isotope compositions. The samples were selected to cover the range of textural varieties of the different rock types in a representative way. The sample localities are shown in Fig. 1b. Additionally, two samples of hydrothermal quartz were analysed for their $\delta^{18}O$ values: sample Q-M is from a centimetre-thick quartz vein and sample Q-D from a cavity containing centimetre-sized euhedral quartz crystals. Both samples were collected from the same locality as sample GM1635.

Minerals were analysed using a JEOL 8900 electron microprobe at the Institut für Geowissenschaften at the Universität Tübingen. For calibration both natural and synthetic standards were used. The beam current was 15 nA and the acceleration voltage was 15 kV. The counting time on the peak was 16 s for major elements, and 30–60 s for minor elements (Mn, Ti, Zr, F, Cl). Background counting times were half of the peak counting times. The peak overlap between the Fe Lβ and F Kα lines was corrected for. To avoid Na migration under the electron beam, feldspar was analysed using a defocused beam of 15 μm diameter. Data reduction was performed using the internal φρZ procedures of JEOL (Armstrong, 1991).

Bulk compositions of coarsely exsolved feldspars and titanomagnetites were recalculated by combining image processing (NIH Image software) of backscattered electron (BSE) images of the exsolved minerals with point analyses of the exsolved phases [see Marks & Markl (2001) for a more detailed description of the technique]. Bulk compositions for each mineral and sample were calculated using 3–5 grains.

Trace element contents were measured by *in situ* laser ablation–inductively coupled plasma-mass spectrometry (LA–ICP-MS) at the EU Large Scale Geochemical Facility (University of Bristol) using a method similar to that described by Halama *et al.* (2002). The precision of trace element concentrations, based on repeated analyses of standards, was approximately ±5%. The detection limit for Li was typically 150–250 ppm, for Rb and Sr 0·1–1 ppm, and for REE $<0{\cdot}1$ ppm.

Whole-rock analyses were performed by standard X-ray fluorescence (XRF) techniques at the Institut für Mineralogie, Petrologie und Geochemie at the Universität Freiburg, using a Philips PW 2404 spectrometer. Pressed powder and Li-borate fused glass discs were prepared to determine contents of trace and major elements, respectively. The raw data were processed with the standard XR-55 software of Philips. Relative standard deviations are $<1\%$ and $<4\%$ for major and trace elements, respectively. Detection limits vary between 1 and 10 ppm, depending on the specific trace element.

Oxygen isotope compositions of powdered whole-rock samples were determined by a conventional method modified after Clayton & Mayeda (1963) and Vennemann & Smith (1990), using BrF_5 as reagent and converting the liberated oxygen to CO_2.

The oxygen isotope composition of hand-picked mineral separates was measured using a method similar to that described by Sharp (1990) and Rumble & Hoering (1994). Between 0·5 and 2 mg of sample were loaded onto a small Pt sample holder and evacuated to a vacuum of $\sim 10^{-6}$ mbar. After prefluorination of the sample chamber overnight, the samples were heated with a CO_2 laser in an atmosphere of 50 mbar of pure F_2. Excess F_2 was separated from O_2 by exchange with KCl held at 150°C. The extracted O_2 was collected on a molecular sieve (13X). Oxygen isotopic compositions were measured on O_2 using a Finnigan MAT 252 mass spectrometer. The results are given in the standard δ-notation, expressed relative to VSMOW in permil (‰). Replicate oxygen isotope analyses of the standards (12 loads of NBS-28 quartz and 10 loads of UWG-2 garnet; Valley *et al.*, 1995) had an average precision of ±0·1‰ for $\delta^{18}O$ ($\pm 2\sigma$ error of the mean). The accuracy of $\delta^{18}O$ values was better than 0·2‰ compared with accepted $\delta^{18}O$ values for NBS-28 of 9·64‰ and UWG-2 of 5·8‰.

For Sr and Nd isotope analyses, about 10 mg of hand-picked mineral separate were spiked with mixed ^{84}Sr–^{87}Rb and ^{150}Nd–^{149}Sm tracers before dissolution under high pressure in HF at 180°C in polytetrafluoroethylene (PTFE) reaction bombs. Rb and Sr were separated in quartz columns containing a 5 ml resin bed of AG50W-X12, 200–400 mesh, equilibrated with

Table 1: Mineralogy of the investigated samples from the Puklen intrusion

Sample	Rock type	Primary magmatic minerals	Secondary, late- to post-magmatic minerals
GM1580	syenite	ol + aug + ilm + mag + alkfsp + am I + ap + zrn	am II + ab + tit
GM1583	syenite	ol + aug + ilm + mag + alkfsp + am I + ap + zrn	am II + ab + tit
GM1586	syenite	ol + aug + ilm + mag + alkfsp + am I + ap + zrn	ab
GM1587	alkali granite	am + ilm + alkfsp + qtz I + ap + zrn	aeg + ab + fl + hem + qtz II + astr
GM1589	syenite	ilm + am I + alkfsp + qtz + zrn	am II
GM1590	syenite	aug + ilm + am I + alkfsp + ap	am II + tit + ab
GM1592	granophyre	ilm + mag + am I + qtz + ap + fl	am II
GM1593	granophyre	aug + ilm + mag + am I + qtz + ap + fl	am II
GM1600	syenite	aug + ilm + am I + alkfsp + qtz + ap + zrn	am II + ab + tit
GM1603	syenite	aug + ilm + am I + alkfsp + qtz + ap + zrn	am II + bio
GM1605	alkali granite	am + ilm + alkfsp + qtz I + ap + zrn	aeg + ab + fl + hem + qtz II + astr
GM1606	alkali granite	am + ilm + alkfsp + qtz I + ap + zrn	aeg + ab + fl + hem + qtz II
GM1608	alkali granite	am + ilm + alkfsp + qtz I + ap + zrn	aeg + ab + fl + hem + qtz II
GM1611	syenite	ol + aug (?) + ilm + alkfsp + ap + zrn	aeg + ab + cc
GM1615	syenite	ol + aug + ilm + alkfsp + am I + ap + zrn	aen + ab + qtz II + cc + $Fe(OH)_x$ + tit
GM1616	syenite	ol + aug + ilm + alkfsp + am I + ap + zrn	aen + ab + qtz II + cc + $Fe(OH)_x$ + tit
GM1620	microgranite	am + mag + alkfsp + qtz + ap + zrn	aeg + ab + astr
GM1625	syenite	aug + mag + am I + alkfsp + ap + zrn	bio
GM1627	microgranite	am + mag + alkfsp + qtz + ap + zrn	aeg + ab
GM1634	syenite	ol + aug + mag + alkfsp + am I + ap	am II + bio
GM1635	syenite	aug + ilm + alkfsp (?) + qtz + am I + ap	aeg-aug + ab + andr + tit + mag + qtz

2·5N HCl. Sm and Nd separation was performed in quartz columns using 1·7 ml Teflon powder coated with HDEHP (di-ethyl hexyl phosphate) as cation exchange medium, equilibrated with 0·18N HCl. All analyses were made by thermal ionization mass spectrometry (TIMS) using a Finnigan MAT 262 system in static collection mode. Sr was loaded with a Ta–Hf activator and measured on a single W filament. Rb, Sm and Nd were measured with a double Re-filament configuration. The $^{87}Sr/^{86}Sr$ ratios were normalized to $^{86}Sr/^{88}Sr = 0{\cdot}1194$, the $^{143}Nd/^{144}Nd$ ratios to $^{146}Nd/^{144}Nd = 0{\cdot}7219$, and the Sm isotopic ratios to $^{147}Sm/^{152}Sm = 0{\cdot}56081$. Repeated analyses of Ames metal (Geological Survey of Canada, Roddick *et al.*, 1992) gave a $^{143}Nd/^{144}Nd$ ratio of $0{\cdot}512142 \pm 22$ ($\pm 2\sigma_m$, $n = 10$) and of the NBS 987 Sr standard yielded a $^{87}Sr/^{86}Sr$ ratio of $0{\cdot}710264 \pm 16$ ($\pm 2\sigma_m$, $n = 8$). Total procedural blanks (chemistry and loading) were <200 pg for Sr and <100 pg for Nd. A decay constant of $1{\cdot}42 \times 10^{-11}$ a^{-1} for ^{87}Rb (Steiger & Jäger, 1977) and of $6{\cdot}54 \times 10^{-12}$ a^{-1} for ^{147}Sm (Lugmair & Marti, 1978) were used. ε_{Nd} values were calculated using present-day CHUR values of 0·1967 for $^{147}Sm/^{144}Nd$ (Jacobson & Wasserburg, 1980) and 0·512638 for $^{143}Nd/^{144}Nd$ (Goldstein *et al.*, 1984). Initial Sr and Nd isotope ratios were calculated for an age of 1170 Ma, on the basis of U–Pb ages on zircons from the Nunarssuit intrusion, which is close to the Puklen complex and consists of similar rock types (Finch *et al.*, 2001). Calculated uncertainty in ε_{Nd} units based on analytical errors is not more than 0·5. The error based on age uncertainty is of the order of 0·5–1·0 ε_{Nd} unit for ages, which are 100 Myr younger or older, depending on the Sm/Nd ratio.

PETROGRAPHY

The following description of the rock types is a brief summary. Detailed and comprehensive petrographic descriptions have been given by Parsons (1972). The mineralogy of the investigated samples is summarized in Table 1. Abbreviations used in the text and figures are given in the Appendix.

Syenite suite

Syenites are highly variable with respect to colour, grain size, texture and modal mineralogy. Most varieties are equigranular; porphyritic types with subhedral feldspar phenocrysts are less common. The syenites are highly variable in quartz content, but

nepheline-bearing syenites do not occur. In some places euhedral centimetre-sized quartz crystals in miarolitic cavities can be found. The dominant matrix feldspar is mesoperthite. In some large feldspar grains, unexsolved cores are still preserved. Some of the quartz-free samples contain interstitial albite. Primary mafic minerals are olivine, clinopyroxene (augite), Fe–Ti oxides, amphibole (amphibole I), apatite and zircon. Olivine, which is now replaced by orange to red iddingsite, is restricted to quartz-free samples. Parsons (1972) noted the rarity of fresh olivine. Subhedral augitic clinopyroxene is grey to green and some grains are strongly zoned. The primary Fe–Ti oxide in most syenites is ilmenite. Some samples show a magmatic two-oxide assemblage of ilmenite and titanomagnetite, and in two samples, titanomagnetite is the only primary Fe–Ti oxide. Primary titanomagnetite is always oxy-exsolved to ilmenite and magnetite in both trellis and less frequently sandwich-type forms [terminology after Buddington & Lindsley (1964)]. Dark brown to dark green amphibole (amphibole I) (Fig. 2a and b) occurs as interstitial crystals or as overgrowths on augite (Fig. 2b). Apatite is found as inclusions in alkali feldspar, augite and amphibole I. Zircon forms small subhedral crystals enclosed in alkali feldspar. In virtually all syenite samples, the primary magmatic phase assemblage is overprinted by a late-stage peralkaline phase assemblage. Augite may show green patches or rims of aegirine-rich pyroxene (Fig. 3). Amphibole I is overgrown by a later pale green amphibole (amphibole II; Fig. 2a) and the primary feldspars developed fine-grained albite along grain boundaries (Fig. 2c).

Two samples without primary quartz (GM1615 and GM1616) contain aenigmatite. Within these samples, augite, ilmenite and amphibole I form clusters in the feldspar matrix. Albite, secondary quartz II and Ca–Fe carbonates are common as interstitial mineral phases. Aenigmatite forms rims around ilmenite (Fig. 2d). Cracks within aenigmatite are filled with fine-grained titanite and Fe-hydroxides. Titanite also occurs along the contact between ilmenite and aenigmatite. Augite close to aenigmatite is converted to bright green aegirine–augite (Fig. 3).

In sample GM1635, a green rim of aegirine–augite has a distinct grain boundary against the primary augite core (Fig. 3b). The rim can be divided into an inner (aegirine–augite I) and outer part (aegirine–augite II). The inner part contains rounded relics of primary augite (white dashed line in Fig. 3b) and shows patchy irregularities in colour. The boundary between inner and outer parts probably marks the former grain boundary of the primary augite (red dashed line in Fig. 3b). The aegirine–augite rim is overgrown by subhedral hydroandradite with oscillatory zoning patterns, which is associated with subhedral titanite and Ti-free magnetite. Primary ilmenite occurs as inclusions within augite or is overgrown by titanite. The matrix consists of recrystallized quartz and albite.

In sample GM1611, primary augite is entirely replaced by aegirine (Fig. 2e), $(\text{calcite–siderite})_{ss}$, quartz and haematite pseudomorphs after former augite. Coarse-grained albite and $(\text{calcite–siderite})_{ss}$ are arranged around aegirine. Neither amphibole I nor amphibole II is present. The matrix feldspar is mesoperthite.

Granophyre

The rock is highly leucocratic and fine grained. It consists mainly of euhedral perthitic alkali feldspar overgrown by graphic intergrowths of quartz and alkali feldspar (Fig. 2f). Mafic minerals are rare and comprise augite, ilmenite, and amphibole I and II. Textures of the mafic minerals are similar to those in syenites. Interstitial zircon and especially fluorite are abundant accessory phases.

Alkali granite

Primary magmatic minerals in this rock are alkali feldspar, quartz, ilmenite and amphibole. Minor minerals and accessories are aegirine, astrophyllite, apatite, zircon, fluorite and titanite. Feldspar is mesoperthitic and graphic intergrowths of quartz and feldspar are common. Grain boundaries between quartz and alkali feldspar may be filled with granular masses of fine anhedral albite (Fig. 2c), in some cases associated with tiny needles of aegirine. Ilmenite occurs as inclusions in amphibole or aegirine. Amphibole is subhedral deep blue to dark grey arfvedsonite. Commonly it is overgrown and replaced by bottle-green aegirine (Fig. 2g). Aegirine also occurs interstitially, forming radially arranged aggregates that are partly associated with astrophyllite (Fig. 2h). Apatite is enclosed in feldspar and in amphibole. Zircon forms small subhedral grains that may be clustered into bigger groups. In some samples, titanite is an interstitial phase. Fluorite occurs as anhedral inclusions in aegirine.

In some samples small veinlets of quartz cut the early magmatic minerals. This feature corresponds to field observations of some quartz veins and lenses of $\sim$10 cm thickness in or close to the granite.

Microgranite

This rock is leucocratic and fine grained. Primary magmatic minerals are alkali feldspar, quartz, magnetite and arfvedsonite. Aegirine occurs as radiating aggregates or overgrows deep blue amphibole. However, in

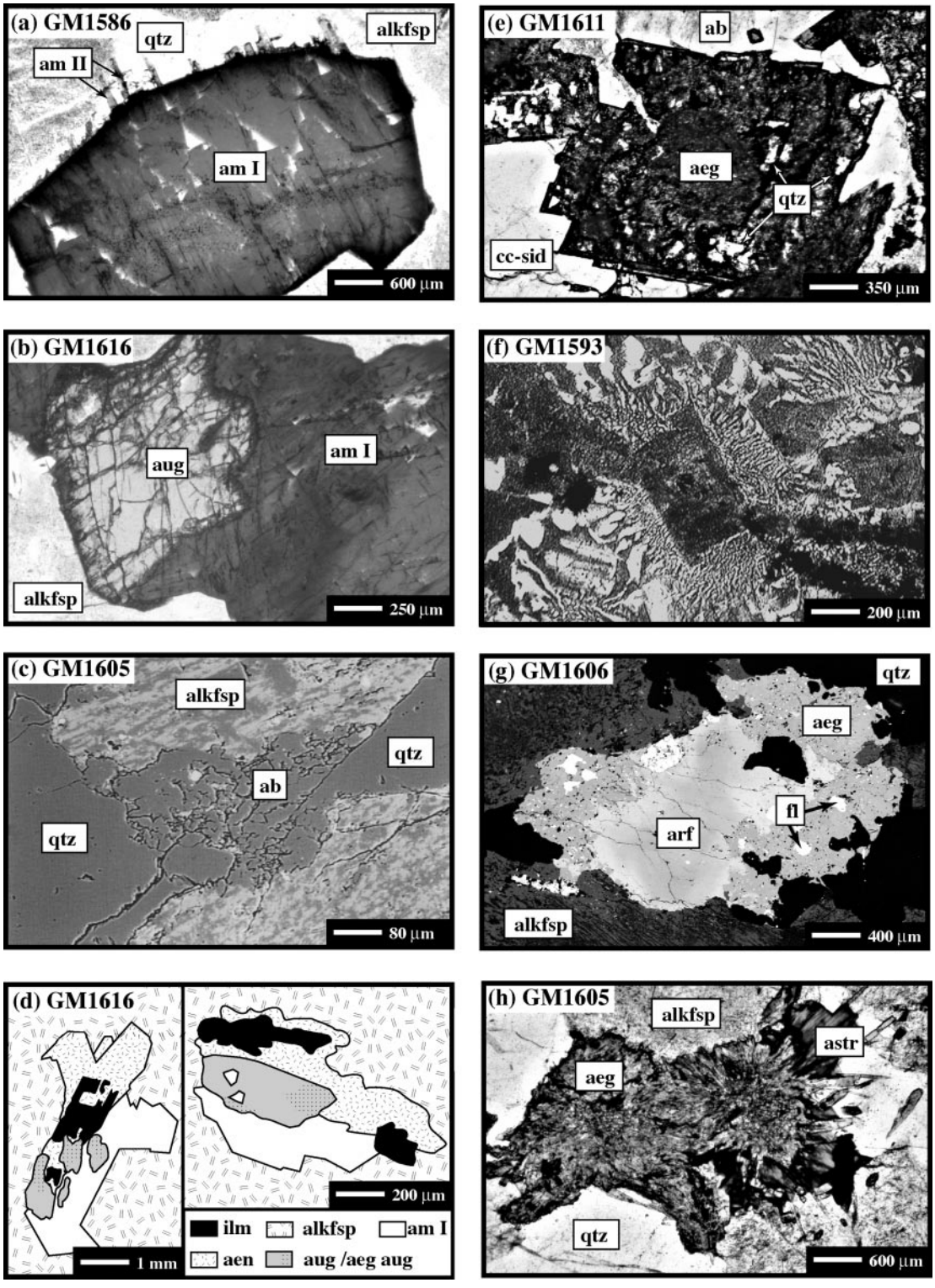

Fig. 2. Photomicrographs (plane-polarized light), BSE images and sketches of mineral textures observed in the Puklen rocks. (a) Autometasomatic ferro-actinolite (am II) overgrowing interstitial ferro-richterite (am I) in syenite. (b) Primary augite, which is overgrown by interstitial amphibole I in syenite. (c) BSE image of granular late-stage albite in granite. (d) Two sketches of aenigmatite textures in syenite. (e) Secondary aegirine with small inclusions of quartz, $(calcite–siderite)_{ss}$ and haematite (not visible). (f) Graphic intergrowths of quartz and alkali feldspar in granophyre. (g) BSE image of arfvedsonite, which is replaced by aegirine in granite. Inclusions of fluorite are also visible. (h) Late-stage, radially arranged aegirine aggregate associated with astrophyllite in granite.

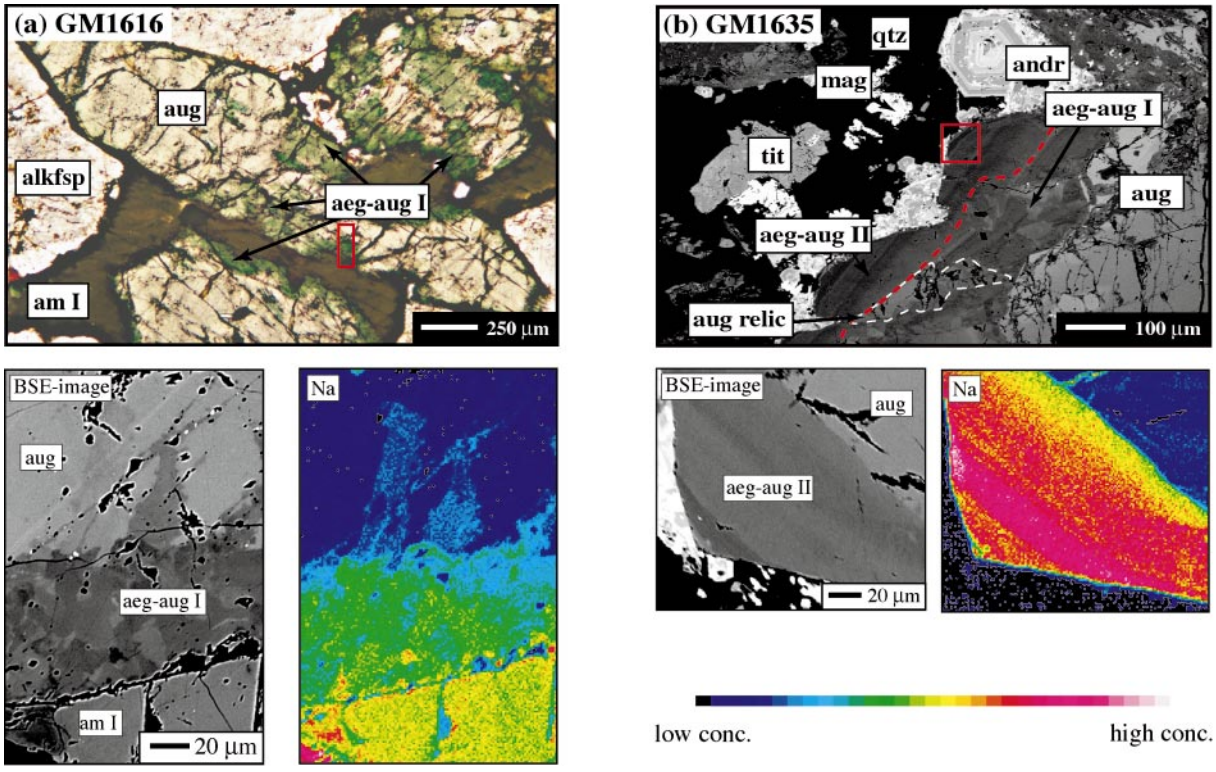

Fig. 3. (a) Top: photomicrograph (plane-polarized light) of augite, which is metasomatized along cracks and grain boundaries by a fluid phase (sample GM1616). Bottom: BSE image (left) and element map for Na (right) of a typical Na-enriched area. (b) Top: BSE image of aegirine–augite II rim around primary augite (sample GM1635). Secondary phases include hydroandradite, titanite, Ti-free magnetite and quartz. The dashed red line represents the assumed former grain boundary of primary augite. The dashed white line outlines a relic of primary augite. Bottom: BSE image (left) and element maps for Na (right) of an aegirine–augite II rim, which shows oscillatory zonation.

the same samples, amphibole may overgrow aegirine, implying that the two mafic minerals crystallized alternately or even may have coexisted in parts of the microgranites. In some of the microgranitic veins, zircon and astrophyllite are remarkably common. The latter forms fringes of small yellow needles around aegirine. Zircon occurs interstitially or as inclusions in quartz. In one of the microgranitic dykes (about 2 cm thick), compositional zoning is marked by the occurrence of amphibole and zircon in the inner parts of the dyke, whereas the margins are rich in aegirine.

RESULTS

Mineral chemistry

Feldspar

Measured and recalculated bulk feldspar compositions of the Puklen rocks are shown in Fig. 4a–c. Some typical analyses are reported in Table 2. Feldspar phenocrysts in syenites are partly chemically zoned and range in composition between $Ab_{74}An_7Or_{19}$ and $Ab_{53}An_2Or_{45}$. Feldspar phenocrysts in samples GM1615 and GM1616 are lower in An component compared with the other syenite samples (Fig. 4a). In one sample (GM1580), early ternary feldspar is essentially unzoned, but shows a strong and steep enrichment of Ab component with almost unchanged An component at the rim (Fig. 4b). The most common matrix feldspar in the syenites is almost Ca-free patchily exsolved alkali feldspar with bulk compositions between $Ab_{69}An_0Or_{31}$ and $Ab_{43}An_0Or_{57}$. Late-stage albite in syenites has nearly end-member composition. The low Ca contents clearly distinguish these fine-grained aggregates from the Ab-rich rims around phenocrysts in sample GM1580 (see above).

Feldspar compositions in granophyres range from $Ab_{57}An_0Or_{43}$ to $Ab_{44}An_0Or_{56}$ and are more Or rich compared with the syenites. In one sample (GM1605) of coarse alkali granite, the composition of the unexsolved core of an alkali feldspar was determined as $Ab_{69}An_4Or_{27}$–$Ab_{65}An_2Or_{23}$ (Fig. 4c). Compositions of matrix feldspars in coarse granites are similar to those in syenites and range between $Ab_{63}An_1Or_{26}$ and $Ab_{49}An_0Or_{51}$. As in syenites, late-stage albite shows almost end-member composition. Feldspar compositions in the microgranites ($Ab_{72}An_1Or_{27}$–$Ab_{49}An_0Or_{51}$) extend the range towards more albite-rich compositions. As in the granophyres, late-stage albite is lacking.

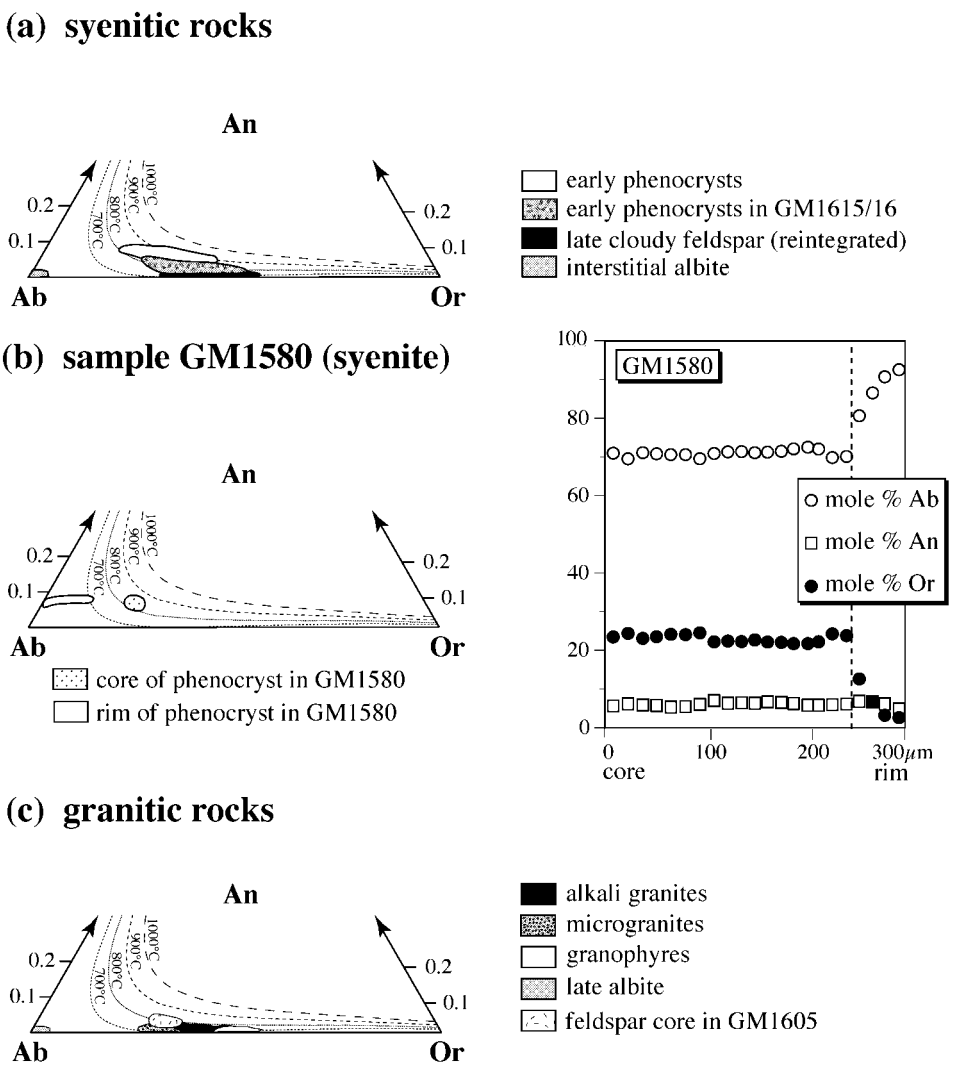

Fig. 4. Feldspar compositions observed in the Puklen rocks. (a) Syenitic rocks. (b) Composition and zoning profile of a ternary feldspar phenocryst in syenite sample GM1580. (c) Granitic rocks. Feldspar solvus after Elkins & Grove (1990).

Olivine

The composition of olivine could not be determined by electron microprobe, as it is altered to red–orange iddingsite. Olivine in such rock types is expected to be fayalite rich (e.g. Stephenson, 1974; Larsen, 1976; Powell, 1978; Upton *et al.*, 1985; Marks & Markl, 2001).

Pyroxene

The primary pyroxene in the syenites and granophyres is augite with >90 mol % quadrilateral (Di + Hed + En + Fs) components (Fig. 5, Table 3). The Na content of the primary augite varies between 0·03 and 0·15 atoms per formula unit (a.p.f.u.) but exceeds in some analyses Fe^{3+}, which was calculated based on stoichiometry (four cations, six oxygens). This indicates the presence of small amounts of the jadeite molecule (up to 6 mol %) in addition to the aegirine component. Some augites show chemical zonation (Fig. 5b). X_{Fe} and Mn increase from core to rim, continuously in some crystals but stepwise in others. The Wo component is more or less constant, Na shows a continuous and smooth enrichment, and Ti decreases. In cracks or rims on augite, the aegirine component rises to ~40 mol % (Fig. 5a). In such areas, augite is enriched in Na, whereas Ca, Mg and Ti are depleted.

In the texture of Fig. 3b, the inner aegirine–augite I shows patchy irregularities in chemical composition. Similar to the other samples, it is enriched in Na and depleted in Ca, Mg and Ti. The outer aegirine–augite II shows oscillatory zoning with respect to Na and other elements and is enriched in Al compared with

Table 2: Representative microprobe analyses of feldspars

Sample:	GM1615	GM1580	GM1580	GM1600	GM1605
Rock type:	syenite	syenite	syenite	syenite	granite
Feldspar type:	phenocryst	phenocryst	ab rim	ab interstitial	phenocryst
wt %					
SiO_2	66·52	65·57	67·81	67·91	65·15
Al_2O_3	18·91	20·48	20·37	20·28	20·25
FeO	0·20	0·15	0·15	0·05	0·09
MnO	0·04	0·02	0·01	0·08	0·20
MgO	0·01	0·00	0·00	0·02	0·01
CaO	0·26	1·06	1·01	0·09	0·84
Na_2O	6·92	7·93	10·57	11·69	7·53
K_2O	6·57	4·22	0·45	0·10	5·16
Total	99·44	98·94	99·88	100·17	99·23
Formulae based on 8 oxygens					
Si	2·99	2·93	2·96	2·96	2·93
Al	1·00	1·08	1·05	1·04	1·07
Mg	0·00	0·00	0·00	0·00	0·00
Fe	0·01	0·01	0·01	0·00	0·00
Mn	0·00	0·00	0·00	0·00	0·01
Ca	0·01	0·05	0·05	0·00	0·04
Na	0·60	0·69	0·89	0·99	0·66
K	0·38	0·24	0·03	0·01	0·30
Sum	5·00	4·99	4·98	5·01	5·01
Ab	61	70	93	99	66
An	1	5	5	0	4
Or	38	25	3	1	30

the primary augite (not shown). In syenite sample GM1611 (Fig. 2e), the chemical composition of the aegirine varies between $Aeg_{72}Di_3Hed_{25}$ and $Aeg_{95}Di_0Hed_5$ and lies within the range observed in the granites (see below).

Pyroxene in coarse granites and microgranites is aegirine with compositions between $Aeg_{76}Di_4Hed_{20}$ and $Aeg_{92}Di_0Hed_8$ (Fig. 5a, Table 3). Aegirine is essentially unzoned and there is no significant compositional difference between aegirine in the coarse granites and in microgranites. Al is the most important minor element; the jadeite component makes up as much as 6 mol %.

Fe–Ti oxides

Table 4 reports some typical analyses of ilmenite and titanomagnetite in the various rock types. The composition of primary ilmenite in syenites varies between $Ilm_{80}Hem_6Pyr_{14}$ and $Ilm_{95}Hem_1Pyr_4$. Recalculated compositions of primary Ti-magnetite grains in syenites range between $Usp_{72}Mag_{28}$ and $Usp_{97}Mag_3$. Such Ti-rich compositions have already been reported from the augite syenite of the Ilímaussaq intrusion (Marks & Markl, 2001). Granophyric samples contain ilmenite with compositions between $Ilm_{84}Hem_5Pyr_{11}$ and $Ilm_{95}Hem_2Pyr_3$.

Ilmenite in coarse granites is rich in MnO and varies between $Ilm_{91}Hem_0Pyr_9$ and $Ilm_{64}Hem_6Pyr_{30}$. The only primary Fe–Ti oxide observed in microgranites is magnetite with Usp contents <5 mol %.

Secondary Fe–Ti oxides in late- to post-magmatic textures are essentially Ti-free magnetite in some syenite samples and end-member haematite in granites.

Amphibole

Amphibole I in syenites is ferro-richteritic to ferro-edenitic in composition (Table 5). X_{Fe} in the entire suite ranges from 0·72 to 0·99. Fluorine (up to 3·5 wt %) always dominates over chlorine ($<0·5$ wt %). Some grains show a pronounced chemical zonation. X_{Fe}, Si, Na and Cl increase from core to rim, whereas Al, Ca and F decrease (Fig. 6a). Amphibole I in fluorite-bearing granophyres is ferro-edenite and essentially

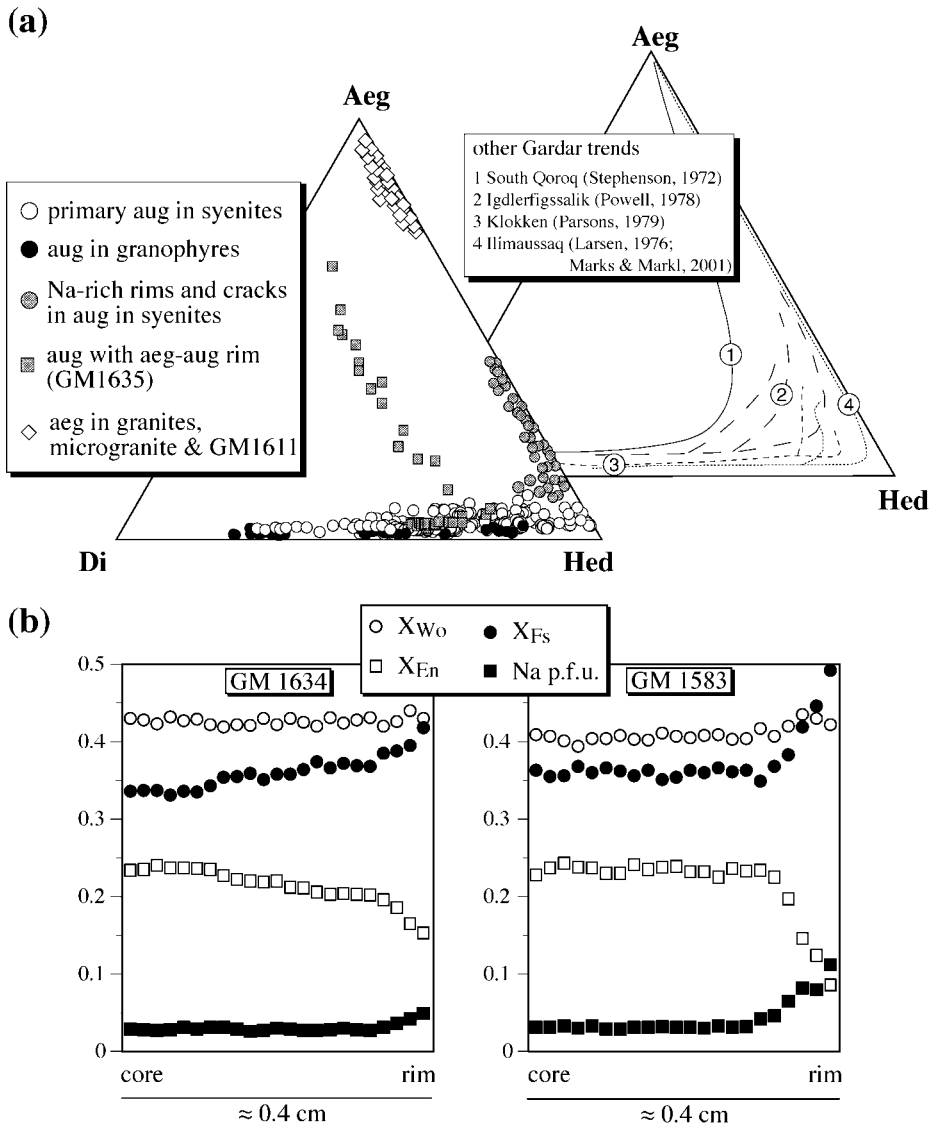

Fig. 5. (a) Clinopyroxene compositional trend in the investigated samples plotted in the ternary system diopside (Di), hedenbergite (Hed) and aegirine (Aeg). Published trends from other Gardar intrusions are shown for comparison. (b) Representative zoning profiles through augite grains in two syenite samples. Formulae are based on four cations and six oxygens. End-member components were calculated after the projection method of Lindsley (1983).

fluorine free. The chlorine content is in the same range as in the syenites.

Amphibole II is a ferro-actinolite. X_{Fe} varies in the same manner as in amphibole I (Table 5). Figure 6a shows a zonation profile starting in the core of an amphibole I crystal and extending into a rim of amphibole II. Compared with amphibole I, these late-stage amphiboles are lower in Na, K, Mn and Ti, and they are also depleted in halogens. Cl is always $<0{\cdot}1$ wt %, and F is below microprobe detection limit.

Amphibole in coarse granites and microgranites is a member of the arfvedsonite–ferro-leakeite series (Table 5). X_{Fe} varies between 0·69 and 0·98. Lithium contents vary from $<0{\cdot}1$ to 1·0 wt % Li_2O. Li is negatively correlated with Fe^{2+} and Al(VI), but positively with Fe^{3+} (Fig. 6b). The main substitution mechanisms for Li in the Puklen arfvedsonites is $Li + Fe^{3+} \leftrightarrow 2(Fe^{2+}, Mg, Mn)$ and $Li + Fe^{3+} \leftrightarrow Al(VI) + Na$. Cl is always $<0{\cdot}05$ wt % whereas F may be up to 3·5 wt %. F is negatively correlated with X_{Fe}.

Aenigmatite

According to the scheme of Kunzmann (1999), the Puklen aenigmatites vary in composition between

Table 3: Representative microprobe analyses of pyroxenes from the various rock types

Sample:	GM1593	GM1600	GM1586	GM1616	GM1616	GM1635	GM1605	GM1608	GM1620
Rock type:	granophyre	syenite	syenite	syenite	syenite	syenite	coarse granite	coarse granite	microgranite
Mineral:	augite	augite	augite	augite	aeg–augite	aeg–augite	aegirine	aegirine	aegirine
wt %									
SiO_2	52·99	49·80	48·85	48·55	48·78	52·05	52·03	51·70	51·18
TiO_2	0·19	0·17	0·43	0·56	0·34	0·02	0·50	0·08	0·13
Al_2O_3	0·70	0·38	0·38	0·23	0·18	0·24	0·37	0·30	0·24
FeO	12·65	24·23	26·56	29·43	29·59	20·08	30·51	31·00	27·32
MnO	0·52	0·59	0·49	0·67	0·66	0·87	0·06	0·19	0·37
MgO	13·61	5·65	2·73	0·81	0·39	4·09	0·10	0·42	1·69
ZrO_2	0·01	0·00	0·01	0·01	0·02	0·00	0·00	0·00	0·00
CaO	19·72	18·78	19·73	19·10	16·59	14·48	0·04	0·90	4·90
Na_2O	0·23	0·35	0·59	0·61	2·49	6·52	13·17	12·24	10·41
Total	100·62	99·95	99·77	99·97	99·04	98·34	96·87	96·82	96·26
Formulae based on 4 cations and 6 oxygens									
Si	1·98	1·98	1·98	2·00	1·99	2·00	2·00	2·00	1·99
Al	0·03	0·02	0·02	0·01	0·01	0·01	0·02	0·01	0·01
Ti	0·01	0·01	0·01	0·02	0·01	0·00	0·01	0·00	0·00
Fe^{3+}	0·01	0·03	0·04	0·01	0·18	0·48	0·95	0·90	0·78
Mg	0·76	0·34	0·17	0·05	0·03	0·23	0·01	0·02	0·10
Fe^{2+}	0·39	0·78	0·86	1·00	0·83	0·17	0·03	0·10	0·11
Mn	0·02	0·02	0·02	0·02	0·02	0·03	0·00	0·01	0·01
Zr	0·00	0·00	0·00	0·00	0·00	0·00	0·00	0·00	0·00
Ca	0·79	0·80	0·86	0·84	0·73	0·60	0·00	0·04	0·20
Na	0·02	0·03	0·05	0·05	0·20	0·49	0·98	0·92	0·79
Sum	4·00	4·00	4·00	4·00	4·00	4·00	4·00	4·00	4·00

Table 4: Representative microprobe analyses and recalculations of Fe–Ti oxides

Sample:	GM1580	GM1603	GM1580	GM1586	GM1593	GM1606	GM1605	GM1620
Rock type:	syenite	syenite	syenite	syenite	granophyre	coarse granite	coarse granite	microgranite
Mineral:	ilm	ilm	usp (calc.)	usp (calc.)	ilm	ilm	ilm	mag
wt %								
TiO_2	47·31	50·38	27·17	32·53	51·63	50·75	51·58	0·06
Al_2O_3	0·00	0·00	0·00	0·03	0·00	0·00	0·00	0·14
FeO	49·25	45·68	68·93	65·20	46·58	42·15	42·62	92·15
MnO	2·52	3·36	1·70	1·26	1·69	5·96	5·32	0·02
MgO	0·01	0·00	0·00	0·00	0·00	0·00	0·00	0·08
Total	99·09	99·42	97·80	99·03	99·90	98·86	99·52	92·45
Formulae based on 3 (2) cations and 4 (3) oxygens for mag (ilm)								
Al	0·00	0·00	0·00	0·00	0·00	0·00	0·00	0·01
Ti	0·90	0·96	0·77	0·92	0·98	0·97	0·98	0·00
Fe^{3+}	0·20	0·08	0·46	0·17	0·04	0·05	0·03	1·99
Mg	0·00	0·00	0·00	0·00	0·00	0·00	0·00	0·00
Fe^{2+}	0·85	0·89	1·72	1·88	0·94	0·84	0·87	1·00
Mn	0·05	0·07	0·05	0·04	0·04	0·13	0·11	0·00
Sum	2·00	2·00	3·00	3·00	2·00	2·00	2·00	3·00

Table 5: Representative microprobe analyses of amphiboles of the various rock types

Sample:	GM1586	GM1615	GM1590	GM1600	GM1600	GM1634	GM1586	GM1606	GM1587	GM1605
Rock type:	syenite	syenite	syenite	syenite	syenite	syenite	syenite	granite	granite	granite
Mineral:	am I	am I	am I	am I	am II	am II	am II	am	am	am
wt %										
SiO_2	45·41	49·27	48·60	44·08	50·15	48·31	50·42	50·67	50·37	51·56
TiO_2	0·20	1·21	1·66	0·83	0·08	0·04	0·06	1·60	1·84	0·31
Al_2O_3	1·64	0·46	1·96	5·00	0·51	0·40	0·74	1·23	1·12	0·75
ZnO	0·00	0·01	0·01	0·02	0·00	0·00	0·00	0·32	0·22	0·18
Li_2O	0·00	0·00	0·00	0·00	0·00	0·00	0·00	0·25	0·20	1·10
FeO	29·60	34·21	32·16	29·51	31·10	34·98	33·42	30·80	30·52	31·94
MnO	0·18	0·55	0·56	0·34	0·40	0·89	0·41	0·47	0·69	0·51
MgO	3·52	0·45	1·26	4·03	3·60	0·55	2·45	1·51	1·32	0·74
CaO	9·81	3·16	5·59	9·62	9·95	10·45	10·54	0·34	0·43	0·64
Na_2O	2·52	6·63	4·69	2·86	0·99	0·47	0·85	8·42	8·43	7·84
K_2O	0·78	1·50	1·35	0·99	0·41	0·16	0·26	1·50	1·58	1·48
ZrO_2	0·00	0·01	0·00	0·01	0·00	0·00	0·00	0·11	0·15	0·08
Cl	0·12	0·02	0·07	0·30	0·02	0·01	0·01	0·01	0·02	0·01
F	3·44	0·00	0·10	1·57	0·00	0·00	0·00	1·70	1·61	0·69
Total	97·22	97·48	98·01	99·15	97·21	96·26	99·15	98·93	98·50	97·84
Formulae based on 23 oxygens										
Si	7·73	7·99	7·92	7·15	7·91	7·89	7·88	7·98	7·98	7·99
Al	0·33	0·09	0·38	0·95	0·09	0·08	0·14	0·23	0·21	0·14
Ti	0·03	0·15	0·20	0·10	0·01	0·01	0·01	0·19	0·22	0·04
Zn	0·00	0·00	0·00	0·00	0·00	0·00	0·00	0·04	0·03	0·02
Li*	0·00	0·00	0·00	0·00	0·00	0·00	0·00	0·16	0·13	0·69
Fe^{3+}	0·00	0·02	0·00	0·00	0·29	0·30	0·20	0·45	0·41	1·14
Mg	0·89	0·11	0·31	0·97	0·85	0·13	0·57	0·35	0·31	0·17
Fe^{2+}	4·21	4·62	4·38	4·00	3·81	4·47	4·17	3·60	3·64	3·00
Mn	0·03	0·08	0·08	0·05	0·05	0·12	0·05	0·06	0·09	0·07
Ca	1·79	0·55	0·98	1·67	1·68	1·83	1·77	0·06	0·07	0·11
Na	0·83	2·08	1·48	0·90	0·30	0·15	0·26	2·57	2·59	2·35
K	0·17	0·31	0·28	0·20	0·08	0·03	0·05	0·30	0·32	0·29
Zr	0·00	0·00	0·00	0·00	0·00	0·00	0·00	0·01	0·01	0·01
Cl	0·03	0·01	0·02	0·08	0·00	0·00	0·00	0·00	0·00	0·00
F	1·85	0·00	0·05	0·80	0·00	0·00	0·00	0·85	0·81	0·34
Sum	16·00	16·00	16·00	16·00	15·08	15·01	15·09	16·00	16·00	16·00

*Li was determined by LA–ICP-MS.

$Aen_{78}Wilk_{18}Rhö_4$ and $Aen_{93}Wilk_4Rhö_3$ (Aenigmatite–Wilkinsonite–Rhönite). The main inferred substitution mechanisms are $Fe^{2+} + Ti^{4+} \leftrightarrow 2\ Fe^{3+}$ and $Ca^{2+} + Al^{3+} \leftrightarrow Na^{+} + Si^{4+}$. With increasing distance from precursor ilmenite, Ca and Al contents decrease, whereas Na, Si and Mn increase.

Carbonates

Carbonates are essentially Mg-free calcite–siderite–rhodochrosite solid solutions. Tiny carbonate inclusions in replaced augite are calcite-rich and vary in composition between $Cc_{97}Sid_2Rhod_1$ and $Cc_{87}Sid_5Rhod_8$. Large interstitial carbonate coexisting with albite is more siderite-rich ($Cc_{72}Sid_{25}Rhod_7$–$Cc_{64}Sid_{30}Rhod_6$).

Andradite

Hydroandradite shows oscillatory zoning (Fig. 3b) and varies in composition between $Andr_{67}Gr_{32}Sp_1Alm_0Py_0$ and $Andr_{91}Gr_6Sp_1Alm_2Py_0$.

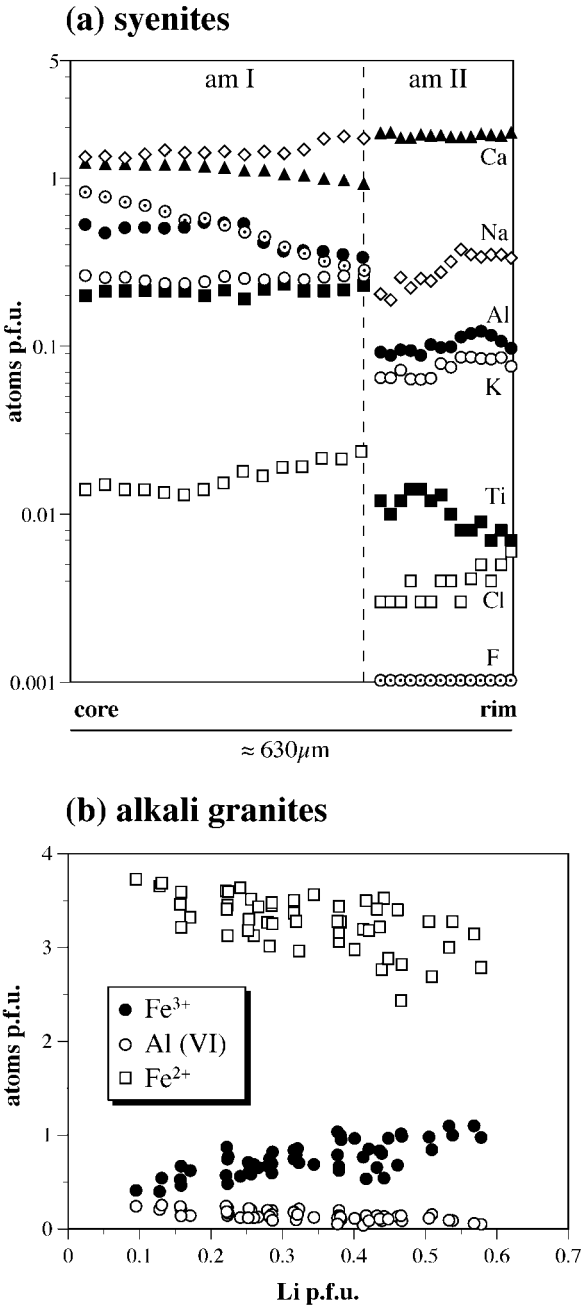

Fig. 6. Amphibole compositions. (a) Zoning profile starting in the core of an interstitial amphibole I through a rim of later amphibole II in syenite. (Note the logarithmic scale of the *y*-axis.) (b) Li vs Fe^{3+}, Al(VI) and Fe^{2+} for the Li-amphiboles in alkali granites. For amphibole I in the syenites and amphibole in the granites, calculated formulae are based on 16 cations and 23 oxygens, assuming a completely filled A site. Formulae for amphibole II in the syenites are calculated after the method of Schumacher, described by Leake *et al.* (1997).

Trace element data for metasomatized augite of sample GM1616

Figure 7 shows selected trace element data for an augite crystal in sample GM1616. On the basis of petrographic observations and mineral compositions it is suggested that late-stage metasomatic fluids have affected the augites of this sample. The unaffected core region (left side of Fig. 7b) has low Rb/Sr ratios between 0·1 and 0·4. In contrast, in the aegirine-rich metasomatized areas (right side of Fig. 7b), both Sr and Rb are enriched by about one and two orders of magnitude, respectively. Rb/Sr ratios increase with increasing Na (i.e. increasing metasomatism) to >1 in metasomatized parts of the crystal. Concentrations of Sm and Nd and Sm/Nd ratios are shown in Fig. 7c for the same analysed points. Both elements are enriched in the metasomatized areas of the crystal, but less significantly than Rb and Sr. Enrichment factors compared with unaffected core regions are about 1·2 for Sm and 1·7 for Nd, resulting in lower Sm/Nd ratios in the metasomatized areas than in unaffected core regions.

Whole-rock geochemistry

Major and trace element analyses of the Puklen rocks are given in Table 6. Some analyses have fairly low totals, which may be attributed to the presence of H_2O^+, CO_2 and halogens, which were not measured. Most samples are peralkaline with an agpaitic index [molar $(Na_2O + K_2O)/Al_2O_3$] between 0·97 and 1·25. The samples have low contents of MgO and CaO, and high concentrations of iron and alkalis. A significant gap in SiO_2 content exists within the Puklen rock series, between syenites and the other rock types (see also Parsons, 1972).

Contents of Al_2O_3, CaO, FeO_t, TiO_2, MnO and P_2O_5 decrease with increasing SiO_2 content from syenites to the other rock types (Fig. 8a). This may suggest fractional crystallization of plagioclase, olivine, augite, magnetite–ilmenite and apatite. However, changes in element concentrations are not always systematic. For example, microgranites, which clearly postdate the coarse alkali granites, have higher contents of CaO and Al_2O_3 than coarse alkali granites.

In general, concentrations of compatible trace elements such as Sc, V, Cr, Co and Ni are low. Of the high field strength elements, Zr is strongly enriched in alkali granites. The concentrations of Zr and Zn correlate positively with the agpaitic index, whereas Sr and Ba concentrations correlate negatively with the agpaitic index (Fig. 8b), which may be attributed to extensive feldspar fractionation.

Oxygen isotope data

Whole-rock and mineral $\delta^{18}O$ values are given in Table 7 and plotted in Fig. 9. The $\delta^{18}O$ values of the syenites span a large range between +4·8 and +6·9‰.

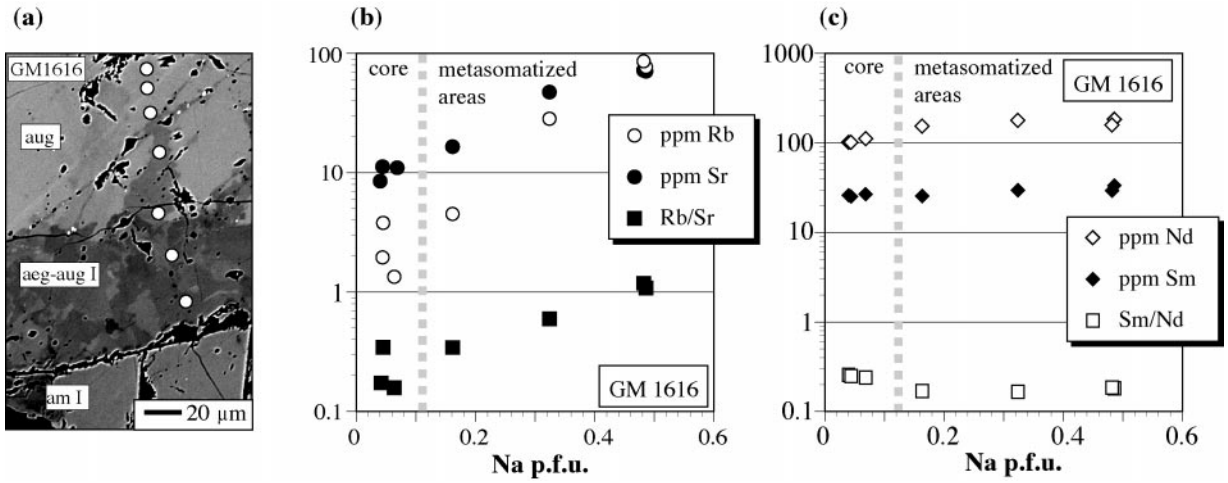

Fig. 7. Trace element data for augite of sample GM1616, which is metasomatized along cracks and grain boundaries by a late-stage fluid phase (compare Fig. 3a). (a) BSE image with data points indicated as white circles. (b) Rb and Sr concentrations plotted against Na p.f.u., which is used as an indicator for increasing metasomatism. The dashed grey line separates measurements in virtually unaffected core regions (left) from metasomatized areas (right) of the same grain. (c) Sm and Nd data for the same data points. Note the logarithmic scale of the *y*-axis.

The values for the two analysed granophyres are +4·6 and +5·0‰, for the three coarse alkali granites are between +5·0 and +5·8‰, and for the two microgranites are +4·9 and +5·5‰.

In syenites and granophyres, the $\delta^{18}O$ values of mineral separates from individual samples decrease in the order quartz–augite–amphibole I–amphibole II. $\delta^{18}O$ values of quartz (+7·9 to +8·1‰), amphibole I (+3·9 to +4·6‰) and amphibole II (+2·5 to +2·8‰) in syenites are rather homogeneous and significantly higher than in the granophyres (+6·4 to 6·7‰, +2·5 to +2·7‰ and +1·0 to +1·7‰, respectively). An explanation for the homogeneous $\delta^{18}O$ values of quartz but the heterogeneous whole-rock $\delta^{18}O$ values will be given later. With the exception of syenite sample GM1616 (+4·7‰), augite in the syenites is also homogeneous, varying between +5·3 and +5·5‰. Augite in the granophyric sample GM1593 (+5·4‰) has a $\delta^{18}O$ value in the range of augite in the syenites. Two separates of perthitic feldspar from syenites have low $\delta^{18}O$ values of +3·5 and +3·9‰.

In coarse alkali granites, $\delta^{18}O$ values decrease from quartz to amphibole to aegirine. The range in measured $\delta^{18}O$ values for all three minerals is large (quartz: +5·1 to +7·3‰; amphibole: +2·2 to + 3·5; aegirine: +0·5 to + 2·0‰) compared with those in the syenites.

In microgranites, the $\delta^{18}O$ values of quartz (+6·7 and +7·2‰) and aegirine (+1·8‰) are in the same range as those in the coarse alkali granites, but amphibole has slightly lower values (+1·7 and +1·9‰). Both quartz and amphibole have significantly lower $\delta^{18}O$ compared with the same minerals in the syenites. The two samples of late-stage quartz veins have $\delta^{18}O$ values similar to quartz in granites (+7·0 and +7·2‰).

Nd isotope data

Thirteen mineral separates from eight samples were analysed for their Sm and Nd concentrations and their Nd isotopic compositions (Table 8). The calculated ε_{Nd} values are all negative and highly variable. The minerals in the syenites cover a fairly large range in ε_{Nd} between −3·8 and −6·4, whereas those in the alkali granites show lower and more variable values between −5·9 and −9·6. Intermediate values of −6·5 for a microgranite amphibole and −7·2 for a granophyre augite were determined. Syenites and the two alkali granites show contrasting Nd isotope behaviour. Although in a particular syenitic sample, augite and amphibole have approximately homogeneous ε_{Nd}, the variability in the Nd isotope composition of the minerals between samples is large. In the two alkali granite samples, the opposite is observed: amphibole and aegirine show almost identical values in the two samples.

Sr isotope data

Six mineral separates from two syenites and two coarse alkali granites were analysed for their Rb and Sr contents and Sr isotopic compositions (Table 8). Rb/Sr ratios of late-stage aegirine (samples GM1605 and GM1606) and metasomatic augite in sample GM1616 are higher compared with those of the primary and unaffected minerals. Augite from sample GM1590 has a highly radiogenic initial $^{87}Sr/^{86}Sr$ of 0·730, whereas augite from sample GM1616 has the lowest value of 0·590. Despite the higher Rb/Sr and $^{87}Rb/^{86}Sr$ ratios of GM1616, the present-day $^{87}Sr/^{86}Sr$ value is low. Amphiboles from alkali granites have low

Table 6: Major and trace element compositions of the Puklen rocks

Rock type:	syenites						alkali granites			granophyres		microgranites	
Sample:	GM1589	GM1590	GM1600	GM1603	GM1611	GM1616	GM1605	GM1606	GM1608	GM1592	GM1593	GM1620	GM1627
wt %													
SiO_2	64·48	59·94	66·79	65·68	61·15	62·11	74·66	74·11	74·21	72·76	70·26	73·38	71·88
TiO_2	0·69	1·10	0·48	0·78	0·66	0·82	0·28	0·28	0·32	0·24	0·31	0·32	0·47
Al_2O_3	14·28	15·09	13·11	13·79	13·04	13·68	11·17	10·26	11·62	12·28	12·52	12·45	13·25
FeO_t	6·69	8·15	3·80	6·46	8·53	8·23	3·30	4·54	3·08	1·66	2·47	2·92	2·76
MnO	0·15	0·17	0·08	0·14	0·17	0·18	0·04	0·06	0·05	0·04	0·05	0·06	0·05
MgO	0·28	0·53	0·42	0·36	0·14	0·18	0·06	0·03	0·06	0·21	0·14	0·20	0·38
CaO	1·48	2·26	1·18	1·76	2·32	2·21	0·33	0·11	0·25	0·45	0·70	0·41	0·98
Na_2O	5·32	5·58	5·02	4·70	6·33	5·44	4·42	4·72	6·40	4·09	4·15	4·71	4·39
K_2O	5·66	5·62	4·56	5·36	4·78	5·26	4·82	4·66	2·22	5·04	5·18	4·84	5·19
P_2O_5	0·08	0·25	0·09	0·14	0·11	0·09	0·01	0·01	0·01	0·03	0·03	0·04	0·09
Total	99·11	98·69	97·44	99·17	97·23	98·20	99·09	98·78	98·22	96·80	95·81	99·33	99·44
A.I.	1·04	1·01	1·01	0·98	1·20	1·07	1·12	1·25	1·11	0·99	0·99	1·04	0·97
ppm													
Sc	5	9	<5	5	<5	<5	<5	<5	<5	<5	<5	<5	<5
V	9	13	17	12	12	9	8	6	14	13	12	13	23
Cr	19	<10	68	<10	<10	64	106	45	155	31	235	<10	<10
Co	<5	<5	<5	<5	<5	<5	<5	<5	<5	<5	<5	<5	<5
Ni	<10	<10	<10	<10	<10	<10	<10	<10	<10	<10	<10	<10	<10
Cu	<5	7	9	8	<5	10	10	6	<5	5	7	5	6
Zn	114	137	69	119	151	151	187	189	209	39	67	71	50
Ga	31	27	21	23	30	31	30	31	28	18	21	20	18
Rb	92	112	121	118	137	119	248	206	79	177	194	174	158
Sr	44	95	165	65	43	31	25	16	26	110	91	88	138
Y	82	74	47	53	74	97	116	66	88	38	68	49	30
Zr	774	483	504	302	572	790	1421	1563	1073	291	510	584	338
Nb	37	30	24	29	32	43	64	71	61	21	38	34	15
Ba	301	752	712	361	121	128	150	136	157	651	405	522	761
Hf	14	9	10	7	9	13	27	27	17	9	13	13	9
Ta	<5	<5	<5	<5	<5	<5	<5	5	<5	<5	<5	<5	<5
Pb	19	18	30	18	18	18	40	40	11	20	28	39	21
Th	7	4	8	4	4	7	15	16	15	14	17	13	5
U	<5	<5	<5	<5	<5	<5	6	5	5	5	5	7	<5

A.I. is agpaitic index [molar $(Na_2O + K_2O)/Al_2O_3$]. Total Fe is expressed as FeO (FeO_t).

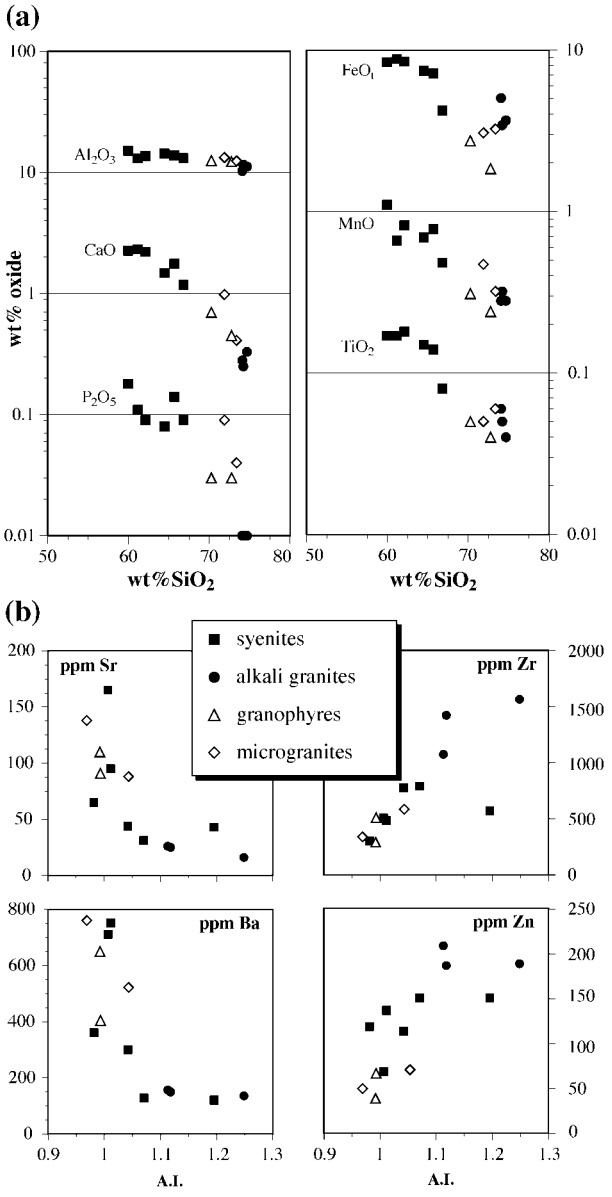

Fig. 8. (a) Major element variation diagrams for the Puklen rocks. SiO_2 is used as *x*-axis. (Note the logarithmic scale of the *y*-axis.) (b) Minor element variation diagrams for the Puklen rocks, with A.I. [agpaitic index; molar ratio of $(Na_2O + K_2O)/Al_2O_3$] as *x*-axis. The syenite sample with the exceptionally high A.I. of 1·2 is sample GM1611, which is a totally metasomatized sample.

initial Sr isotope ratios between 0·699 and 0·696. Late-stage aegirine has even lower values of 0·642–0·631. If ages younger than 1170 Ma are assumed, the calculated initial Sr ratios change only slightly. Only ages younger than ~900 Ma, which are not known from the Gardar Province (Upton & Emeleus, 1987), lead to geologically realistic initial Sr ratios of >0·700–0·703 for depleted sources or >0·703 for isotopically enriched sources (Bulk Earth at 1170 Ma = 0·703). This indicates that the calculated low initial Sr ratios are not an effect of a wrong age assumption, but reflect disturbance of the Rb–Sr system.

CONDITIONS DURING THE MAGMATIC STAGE

Based on fluid inclusion studies (Konnerup-Madsen & Rose-Hansen, 1984; Markl *et al.*, 2001) and on the reconstruction of the sedimentary and extrusive igneous overburden (Upton, 1962; Harry & Pulvertaft, 1963; Poulsen, 1964; Emeleus & Upton, 1976) the pressure of emplacement of the Ilímaussaq complex was estimated to be ~1 kbar. In the lack of better estimates, we use this value as an approximation for the Puklen complex as well.

Syenites and granophyres

Temperature and silica activity

The composition of early ternary feldspar phenocrysts in some syenite samples can be used to constrain near-liquidus conditions in the parental melt. The minimum crystallization temperature of the microperthites was determined by Parsons (1972) to be in excess of 715°C. Figure 4 shows feldspar compositions plotted on the temperature-dependent feldspar solvus after Elkins & Grove (1990). Estimated minimum temperatures range from 750° to ~950°C.

Equilibria between olivine, pyroxene and melt constrain silica activity of the olivine-bearing samples, which were originally quartz-free. Unfortunately, no primary olivine was preserved in the investigated samples. The QUILF program (Andersen *et al.*, 1993) calculates equilibria involving olivine, augite, quartz, magnetite and ilmenite, and was used to estimate the composition of olivine in equilibrium with the measured augite at temperatures between 750° and 950°C. Detailed information on the theory and application of QUILF has been given by Frost & Lindsley (1992), Lindsley & Frost (1992) and Marks & Markl (2001). Calculated olivine compositions range from $Fa_{67}Fo_{31}La_2$ to $Fa_{96}Fo_3La_1$. Because this range is similar to that for olivines from other augite syenites of the Gardar Province (Stephenson, 1974; Larsen, 1976; Powell, 1978; Upton *et al.*, 1985; Marks & Markl, 2001) we believe that these calculations are reliable and can be used to estimate silica activity for these samples.

Calculated silica activities are based on the reference state of pure quartz at *P* and *T*. Silica activity evolved systematically from ~0·70 in the syenite samples

Table 7: Oxygen isotope compositions of whole-rock samples and mineral separates from the Puklen intrusion ($\delta^{18}O$ values given in ‰)

Sample	Whole rock	qtz	aug	aeg	am I	am II	altered fsp
GM1589	4·8	7·9	—	—	4·1	2·8	3·9
GM1590	5·8	—	5·5	—	4·3	2·5	—
GM1600	5·9	8·1	5·5	—	3·9	2·5	3·5
GM1603	6·9	8·1	5·3	—	4·6	2·7	—
GM1611	5·8	—	—	0·2	—	—	—
GM1616	6·5	8·0 (qtz II)	4·7	—	4·4	—	—
GM1605	5·5	7·3	—	1·2	2·2	—	—
GM1606	5·8	7·1	—	2·0	3·5	—	—
GM1608	5·0	5·1	—	0·5	3·3	—	—
GM1592	5·0	6·7	—	—	2·5	1·7	—
GM1593	4·6	6·4	5·4	—	2·7	1·0	—
GM1620	4·9	6·7	—	1·8	1·7	—	—
GM1627	5·5	7·2	—	—	1·9	—	—
Q-D	—	7·0	—	—	—	—	—
Q-M	—	7·2	—	—	—	—	—

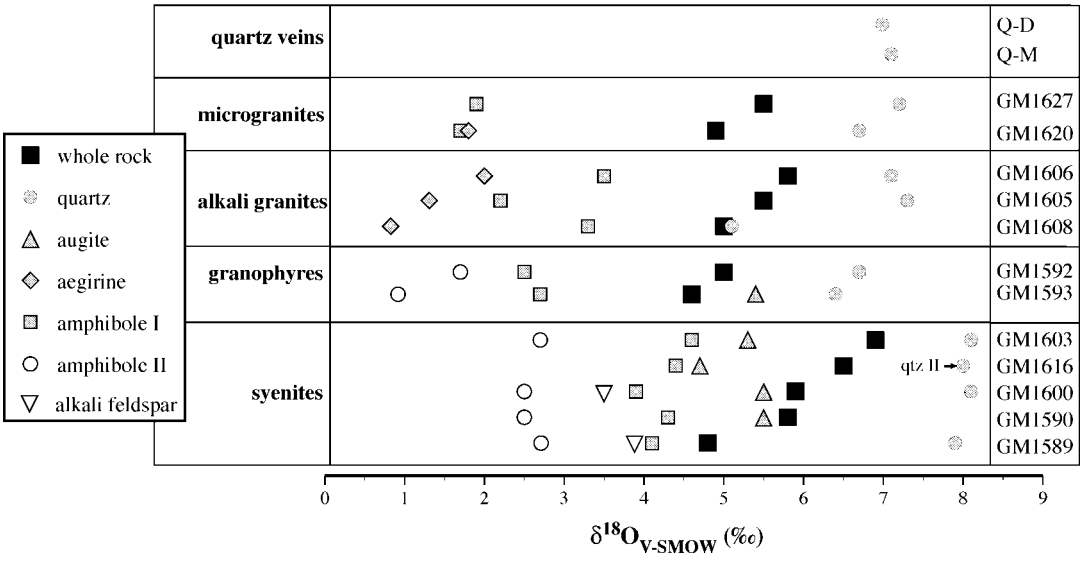

Fig. 9. Oxygen isotope composition of whole-rock samples and mineral separates of the Puklen complex.

with the lowest X_{Fe} in augite to 0·98 in those that contain nearly end-member hedenbergite (Fig. 10). This systematic relationship between X_{Fe} in augite and calculated silica activity in the olivine-bearing syenites indicates that an originally quartz-undersaturated melt evolved by fractionation of olivine, augite and Fe–Ti oxide along a displaced FMQ buffer towards quartz saturation. All other syenites and granites are quartz bearing but lack olivine. The above-mentioned trend of the quartz-free samples (Fig. 10) is not applicable to the quartz-bearing ones. In contrast to what one would expect in a closed system, the quartz-bearing syenites do not contain the Fe–Mg silicates with the highest X_{Fe}, but quartz-bearing syenites show the same range of X_{Fe} in augite as quartz-free samples.

Oxygen fugacity

Oxygen fugacity (f_{O_2}) was calculated from equilibria among Fe–Ti oxides and Fe–Mg silicate minerals

Table 8: Rb–Sr and Sm–Nd data for mineral separates of the Puklen complex

Sample	Rock type	Mineral	Rb	Sr	Rb/Sr	$^{87}Rb/^{86}Sr$	$^{87}Sr/^{86}Sr$	$^{87}Sr/^{86}Sr_i$	Sm	Nd	Sm/Nd	$^{147}Sm/^{144}Nd$	$^{143}Nd/^{144}Nd$	$^{143}Nd/^{144}Nd_i$	ε_{Nd}
			(ppm)			(ppm)			(ppm)	(ppm)					
GM1589	syenite	am II							32·07	145·5	0·2204	0·1332	0·511881(07)	0·510858	−5·3
GM1590	syenite	aug	7·06	18·02	0·392	1·138	0·749407(10)	0·73035	39·56	201·6	0·1962	0·1186	0·511787(08)	0·510876	−4·9
GM1590	syenite	am I							19·97	80·90	0·2469	0·1492	0·512037(09)	0·510891	−4·6
GM1600	syenite	am I							50·20	213·2	0·2355	0·1424	0·511895(07)	0·510801	−6·4
GM1600	syenite	am II							21·86	100·9	0·2167	0·1310	0·511806(09)	0·510800	−6·4
GM1616	syenite	aug	19·22	7·59	2·532	7·330	0·712627(10)	0·58982	44·30	205·1	0·2160	0·1306	0·511938(10)	0·510935	−3·8
GM1616	syenite	am I							22·26	120·7	0·1844	0·1115	0·511749(10)	0·510893	−4·6
GM1605	alkali granite	am	30·77	75·16	0·409	1·186	0·719392(13)	0·69953	16·42	79·43	0·2067	0·1250	0·511781(09)	0·510821	−6·0
GM1605	alkali granite	aeg	19·22	10·17	1·890	5·481	0·734249(10)	0·64242	23·21	82·01	0·2830	0·1711	0·511973(08)	0·510659	−9·2
GM1606	alkali granite	am	32·37	62·57	0·517	1·499	0·721153(09)	0·69604	17·82	90·43	0·1971	0·1191	0·511742(10)	0·510827	−5·9
GM1606	alkali granite	aeg	29·41	12·98	2·266	6·580	0·740842(09)	0·63061	37·67	132·5	0·2843	0·1720	0·511958(09)	0·510637	−9·6
GM1620	microgranite	am							21·72	110·4	0·1967	0·1189	0·511710(7)	0·510797	−6·5
GM1593	granophyre	aug							64·59	327·5	0·1972	0·1192	0·511673(8)	0·510757	−7·2

Errors of measured $^{87}Sr/^{86}Sr$ and $^{143}Nd/^{144}Nd$ are given as 2σ values and are indicated in parentheses. Initial $^{87}Sr/^{86}Sr$, $^{143}Nd/^{144}Nd$ and ε_{Nd} are recalculated for 1170 Ma.

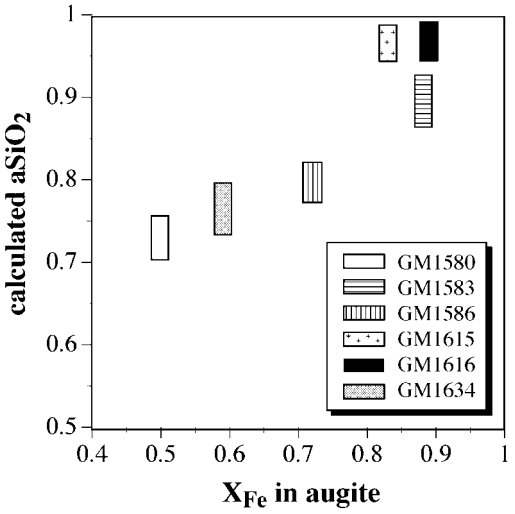

Fig. 10. X_{Fe} in augite vs calculated a_{SiO_2} for samples lacking primary quartz.

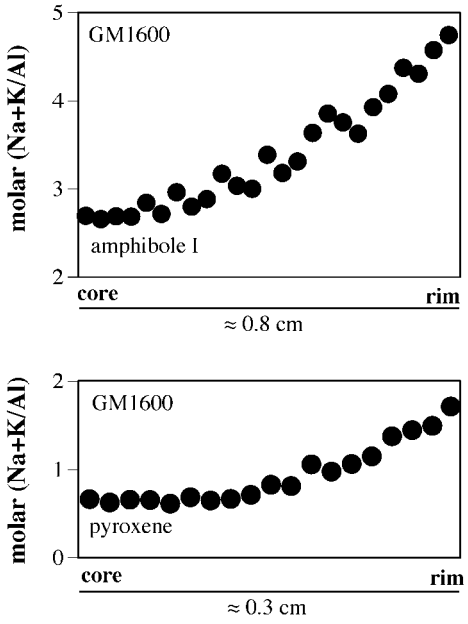

Fig. 11. Profiles from core to rim in pyroxene and amphibole I illustrating the observed increase of molar (Na + K)/Al ratio.

(olivine, augite) using the QUILF program (Andersen *et al.*, 1993). For each sample, calculations were performed for the whole compositional range observed and consequently they yielded a range of f_{O_2} values. Estimated f_{O_2} is always below the synthetic FMQ buffer and varies between 0·8 and 2·3 log units below the FMQ buffer. These and even more reduced conditions seem to be typical for the Gardar syenites (Powell, 1978; Marks & Markl, 2001). Oxygen fugacity in granophyres was estimated to be around or slightly above FMQ at temperatures between 650° and 750°C.

Granites

Temperature

In coarse granites, the rarely preserved homogeneous cores of alkali feldspar indicate minimum temperatures of 750°C (Fig. 4c). The upper stability limit for F-free arfvedsonite is ~700°C (Bailey, 1969). F-rich arfvedsonite is an early liquidus phase in the Puklen granites and F is expected to increase the thermal stability of arfvedsonite significantly because experimental data for richteritic compositions (Gilbert & Briggs, 1974) show a difference in the F and OH stabilities of ~300°C in the low-pressure range. Thus, the crystallization of the magmatic assemblage of the granites occurred at temperatures ≥750°C.

Oxygen fugacity

The only constraint on oxygen fugacity for the magmatic stage of the coarse granites is the occurrence of arfvedsonite. End-member arfvedsonite is stable only at conditions below the synthetic FMQ buffer (Bailey, 1969).

LATE-STAGE PROCESSES IN SYENITES

Formation of aegirine–augite and aenigmatite in syenites

Crystallization of anhydrous minerals such as alkali feldspar, olivine, augite and Fe–Ti oxides under relatively reduced conditions (see above) led to the enrichment of Na, Fe, Si, halogens and H_2O in the residual melt. As a result of increasing H_2O activity, amphibole I began to crystallize as a late magmatic phase. Enrichment of Na and depletion of Al during fractionation is also indicated by the rise of (Na + K)/Al ratio from core to the rim in augite and amphibole (Figs 6a and 11). Upon reaching fluid saturation, a fluid phase (presumably H_2O–CO_2) must have been exsolved, which is suggested by the formation of carbonate minerals. Based on petrographical observations that late- to post-magmatic reactions mainly took place along cracks or grain boundaries and carbonates precipitated at the same time, we conclude that this fluid phase was responsible for these reactions. Because one of the most important replacement textures in our samples is the growth of aegirine at the expense of augite (Fig. 3), we assume this fluid phase was very probably Na dominated. The replacement reaction can be described as follows:

$$4CaFeSi_2O_6 + 4Na^+ + O_2 + 2H_2O \rightarrow 4NaFeSi_2O_6 + 4Ca^{2+} + 4OH^-. \quad (1)$$

The Ca released led to the formation of ferro-actinolite (amphibole II), other secondary Ca-silicates and, in some places, interstitial $(\text{calcite–siderite})_{ss}$. For example, the texture in Fig. 2e (sample GM1611) may be modelled by the schematic reaction

$$4CaFeSi_2O_6 + 2Na^+ + 2OH^- + O_2 + 4CO_2 \rightarrow 2NaFeSi_2O_6 + 4CaCO_3 + 4SiO_2 + Fe_2O_3 + H_2O. \quad (2)$$

During these replacement reactions, the fluid composition changed. This can be inferred in sample GM1635, where the oscillatory zoning patterns in aegirine–augite II (Fig. 3b) suggest discontinuous changes of fluid composition. This might be caused by the complex interplay of dissolution of augite and precipitation of aegirine–augite and the several Ca phases involved.

The formation of aenigmatite at the expense of ilmenite was observed in the two samples (GM1615 and GM1616) showing most extensive growth of Na-pyroxene (Figs 2d and 5a). The following schematic reaction describes this process:

$$4FeTiO_3 + 20CaFeSi_2O_6 + 12Na^+ + 12OH^- + O_2 + 20CO_2 \rightarrow 4Na_2Fe_5TiSi_6O_{20} + 4NaFeSi_2O_6 + 20CaCO_3 + 8SiO_2 + 6H_2O. \quad (3)$$

The formation of aegirine–augite and/or aenigmatite indicates an increased oxidation state of the late-magmatic fluid compared with the early magmatic stage and high amounts of Na dissolved in the fluid. An inverse relationship between aenigmatite and Fe–Ti oxides is often observed (e.g. Marsh, 1975; Larsen, 1977; Grapes *et al.*, 1979; Ike, 1985; Birkett *et al.*, 1996) and led Nicholls & Carmichael (1969) to postulate the existence of a so-called 'non-oxide' field for quartz-saturated systems in T–f_{O_2} space where aenigmatite and aegirine coexist in the absence of Fe–Ti oxides. This non-oxide field is shown in Fig. 12 (grey field) and is bounded by the labelled reactions (a)–(c). It should be noted that reaction curves in Fig. 12 are for constant unit activities of aegirine, magnetite, ilmenite, aenigmatite and sodium disilicate. Following Nicholls & Carmichael (1969), point A in Fig. 12 represents the intersection of reactions (a)–(c) for an aegirine activity of 0·5, and the dashed line indicates the intersection of reactions (a) and (b) depending on the activity of sodium disilicate. Incorporation of Fe^{3+} into aenigmatite shifts reaction (a) to more oxidized conditions and thus expands the non-oxide field to the vicinity of the haematite–magnetite (HM) buffer curve. In summary, the formation of aenigmatite and stabilization of aegirine–augite in some of the Puklen syenites indicates an increase of oxygen fugacity as a consequence of cooling (curved arrow in Fig. 12).

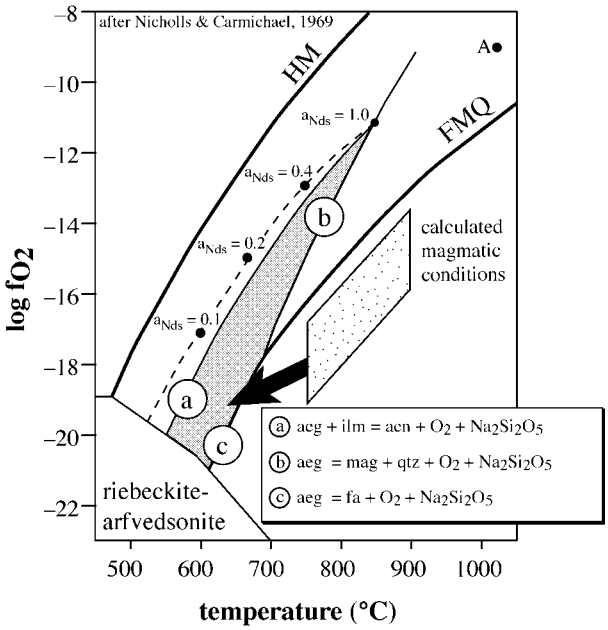

Fig. 12. Stability field of aenigmatite (grey) in a log f_{O_2}–T diagram (after Nicholls & Carmichael, 1969). Stippled field indicates calculated magmatic conditions for some syenites. The curved black arrow describes the formation of aenigmatite in samples GM1615 and GM1616. Point A represents the intersection of the labelled reactions (a)–(c) for an aegirine activity of 0·5, and the dashed line indicates the intersection of reactions (a) and (b) depending on the activity of sodium disilicate. (See text for further explanation.)

Formation of late-stage Ca-minerals in syenites

Replacement of early magmatic Ca-bearing minerals in syenites by late-stage Na-rich minerals led to the release of Ca into the fluid phase and subsequently to the formation of the secondary Ca-bearing minerals ferro-actinolite, $(\text{calcite–siderite})_{ss}$, andradite and titanite. In some samples Ti-free magnetite and quartz are associated with these minerals. Three associations can be distinguished:

(1) $(\text{calcite–siderite})_{ss}$ + titanite + magnetite + quartz;
(2) titanite + hydroandradite + magnetite + quartz;
(3) ferro-actinolite.

Temperature constraints

Carbonate-bearing samples GM1615 and GM1616. Large interstitial Fe-rich carbonates associated with aenigmatite in samples GM1615 and GM1616 were used for solvus thermometry after Goldsmith *et al.*

(1962) and the re-evaluation of Anovitz & Essene (1987). The inferred minimum temperatures for these compositions are not well constrained and range between 650° and 750°C depending on the solvus used. However, these temperatures probably mark the beginning of fluid activity at relatively high temperatures.

Sample GM1611. Carbonates that were found as tiny inclusions in completely metasomatized augite in sample GM1611 indicate minimum temperatures as low as 360–320°C and are better constrained because the solvus curve for such Fe-poor compositions is reasonably well determined (Anovitz & Essene, 1987).

Carbonate-free samples. The upper stability limit of ferro-actinolite (at 1 kbar) has been experimentally determined by Hellner & Schürman (1966) to be about 550–600°C. This is the maximum temperature for the beginning of amphibole II formation during cooling.

The above-mentioned temperature constraints indicate that the formation of secondary Ca minerals occurred within a wide temperature range starting at temperatures close to the magmatic stage of ~750°C and continuing down to temperatures of ~300°C.

Ca-mineral constraints on f_{O_2} *and* a_{CO_2}

Although the principal process of replacement of an early Ca-bearing assemblage by a late Na-bearing one appears to be the same in all samples, the secondary Ca-mineral assemblages are not. We assume that local variations in f_{O_2}, a_{H_2O} or a_{CO_2} were responsible for this. To investigate this, we calculated an f_{O_2}–a_{CO_2} diagram in the Ca–Fe–Si–O–H–C system involving hedenbergite, magnetite, andradite (as an approximation for hydro-andradite), ferro-actinolite, calcite, quartz, CO_2 and H_2O using the GEOCALC software of Berman *et al*. (1987) and Lieberman & Petrakakis (1990) and the database of Berman (1988). New thermodynamic data for ferro-actinolite (Ghiorso & Evans, 2002) were added to this database. A set of isothermal log f_{O_2}–log a_{CO_2} diagrams was calculated from 300° to 600°C. Magnetite was regarded as a pure end-member in accordance with microprobe analyses. For the calculation of end-member component activities we used the solution models of Holland (1990) for hedenbergite and Cosca *et al*. (1986) for andradite. For calcite and ferro-actinolite, a 'mixing on site' model was used. As an example, the topologic relations for reactions among these minerals are shown for 500°C in Fig. 13. Between 300° and 600°C the topologic relations between reactions are similar but the position of the invariant point [Fe-Act] shifts with falling temperature from log f_{O_2} (600°C) = −22 to log f_{O_2} (300°C) = −38 and from log a_{CO_2} = −0·3 to −2·4 (black dots and dashed lines in Fig. 13). However, it is important to note that the position of the invariant point relative to the FMQ buffer is generally independent of temperature and lies at about ΔFMQ = +1 log unit at all temperatures. The f_{O_2}–a_{CO_2} diagram can be used to interpret the various Ca-mineral assemblages, as follows:

(1) the occurrence of andradite in sample GM1635 formed by oxidation of hedenbergite points to a fluid phase with a_{CO_2} < 0·25 (log a_{CO_2} < −0·6) (grey area in Fig. 13) if a temperature of 500°C is assumed. Oxygen fugacity in this rock increased from magmatic values (ΔFMQ = −1 to −2) to above ΔFMQ = +1.
(2) The two aenigmatite- and carbonate-bearing samples GM1615 and GM1616 indicate even higher f_{O_2} and a_{CO_2} values (stippled pattern in Fig. 13).
(3) Ferro-actinolite-bearing (amphibole II) samples were less oxidized and had lower a_{CO_2} (dotted pattern in Fig. 13) or—if oxygen fugacity was higher than in sample GM1635—they coexisted with a fluid phase unusually rich in CO_2, which is considered unlikely.

Occurrence of titanite

In the two samples GM1615 and GM1616 titanite occurs along grain boundaries between ilmenite and aenigmatite [see reaction (3)] and as fine-grained fillings of small cracks within aenigmatite. These textures indicate that titanite formed at the expense of aenigmatite:

$$\mathrm{Ca^{2+} + Na_2Fe_5TiSi_6O_{20} + O_2 + 2OH^- \rightarrow CaTiSiO_5 + 2NaFeSi_2O_6 + SiO_2 + Fe_3O_4 + H_2O.} \quad (4)$$

This reaction separates a more oxidized titanite–aegirine–magnetite–quartz assemblage from a more reduced hedenbergite–aenigmatite assemblage.

In the andradite-bearing sample GM1635, titanite coexists with Ti-free magnetite and quartz (Fig. 3b) as an overgrowth on ilmenite. This can be expressed by the classical reaction (Wones, 1989)

$$\mathrm{3CaFeSi_2O_6 + 3FeTiO_3 + O_2 \rightarrow 3CaTiSiO_5 + 3SiO_2 + 2Fe_3O_4.} \quad (5)$$

Thus, similar to the formation of aegirine–augite and aenigmatite, the occurrence of titanite together with magnetite and quartz implies an increase in oxygen

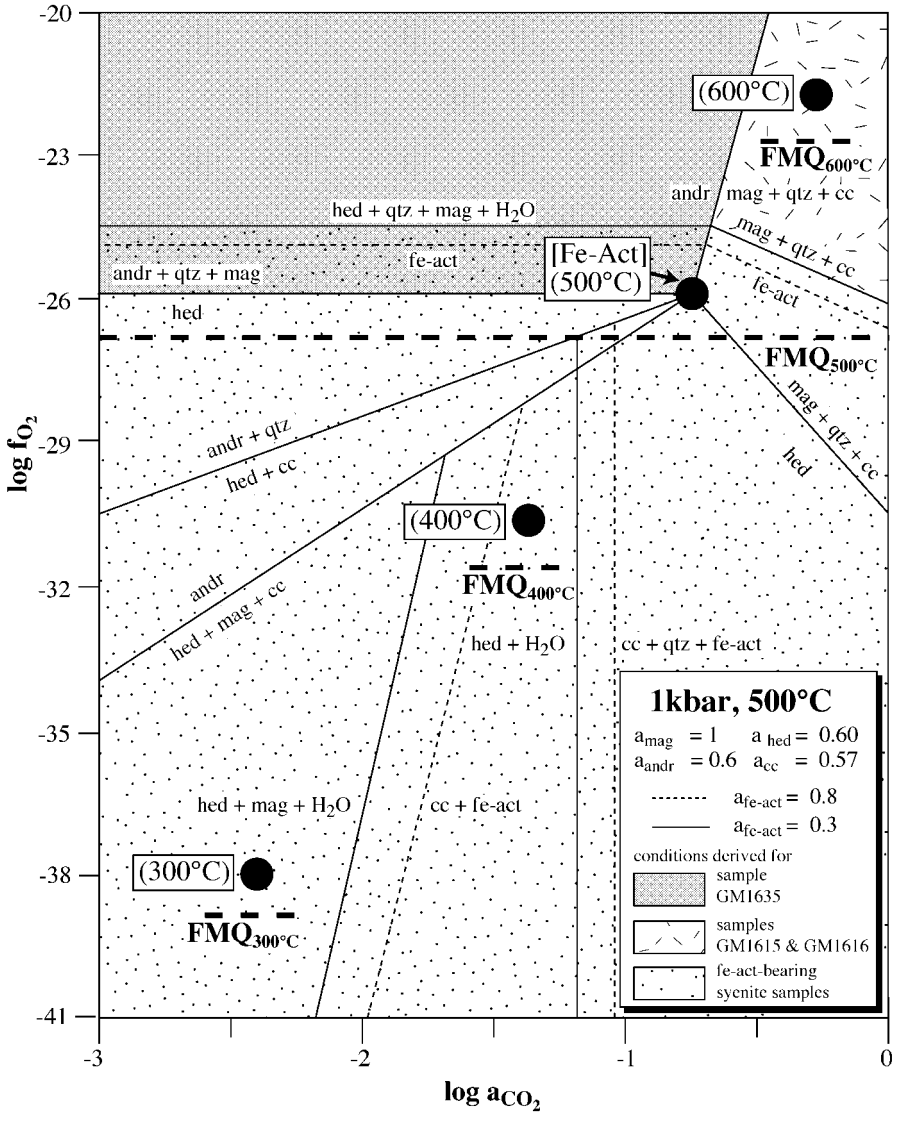

Fig. 13. Log f_{O_2}–log a_{CO_2} diagram (1 kbar) for the system Ca–Fe–Si–O–H–C involving hedenbergite, magnetite, quartz, ferro-actinolite, andradite and calcite. •, position of the invariant point [Fe-Act]; bold dashed lines show the position of the FMQ buffer curve at specified temperatures. The grey, dashed and stippled fields represent the inferred conditions of formation of secondary Ca-mineral assemblages for syenite samples. (See text for further explanation.)

fugacity above the FMQ buffer during sub-solidus cooling.

SIGNIFICANCE OF Li-AMPHIBOLES IN PERALKALINE GRANITES

Similar to Mn, Zn or Zr, Li can be an important component in igneous alkali amphiboles, especially in peralkaline granites (Hawthorne *et al.*, 1993, 1994). Compared with other published data (e.g. Bailey *et al.*, 1993; Hawthorne *et al.*, 2001) Li contents in amphiboles of the Puklen granite (0·1–1·0 wt % Li_2O) are relatively high, but variable. Comparison with the detailed studies of Hawthorne *et al.* (1993, 1994, 2001) shows that the dominant substitution mechanism for Li in the alkali amphiboles of the Puklen peralkaline granite is $^{M3}Fe^{2+} + Fe^{2+} \leftrightarrow {}^{M3}Li + Fe^{3+}$, giving rise to the ideal end-member ferro-leakeite. The Puklen amphiboles contain up to 60 mol % of this component.

Strong & Taylor (1984) distinguished two compositional trends in amphibole from silica-saturated peralkaline igneous rocks. A magmatic to subsolidus trend is characterized by a change in composition from barroisite to richterite to arfvedsonite. The most important substitution here is $^{[4]}AlCa \leftrightarrow SiNa$.

This substitution involves amphiboles with full A sites and this trend is proposed to occur under reducing conditions. Second, the so-called oxidation trend reaches riebeckite composition and takes place under the influence of oxidizing fluids. This also produces amphiboles with vacancies on the A site. The $Fe^{3+}/(Fe^{3+} + Fe^{2+})$ ratio of the two end-members of both trends are 0·20 and 0·40, respectively. As discussed by Hawthorne *et al.* (1993), the incorporation of Li by the mechanism mentioned above increases the $Fe^{3+}/(Fe^{3+} + Fe^{2+})$ ratio from 0·20 in Li-free arfvedsonite to 0·50 in ferro-leakeite, which is even more oxidized than the oxidation trend of Strong & Taylor (1984). The relatively high $Fe^{3+}/(Fe^{3+} + Fe^{2+})$ ratios and high Li contents found in the Puklen arfvedsonites imply an extension of the stability field for these amphiboles to higher oxygen fugacities—even above the FMQ buffer—compared with Li-free arfvedsonite, suggesting that these amphiboles presumably crystallized above the FMQ buffer.

LATE-STAGE FORMATION OF AEGIRINE IN PERALKALINE GRANITES

The formation of aegirine in the Puklen peralkaline granites is a late-stage process and is a well-known phenomenon in peralkaline granites. Most commonly, primary arfvedsonite is replaced by granular aegirine (Fig. 2g), which shows many small inclusions of quartz, fluorite and haematite. This can be described by the following reaction:

$$Na_3Fe_5Si_8O_{22}(OH)_2 + O_2 \rightarrow 3NaFeSi_2O_6 + Fe_2O_3 + 2SiO_2 + H_2O. \quad (6)$$

Inclusions of fluorite in aegirine are attributed to the release of Ca and F during decomposition of Ca- and F-bearing arfvedsonite and represent an important distinction from the syenites. Some textures indicate the formation of aegirine at the expense of magmatic ilmenite:

$$4FeTiO_3 + 8SiO_2 + 4Na^+ + O_2 + 6H_2O \rightarrow 4NaFeSi_2O_6 + 4Ti^{4+} + 12OH^-. \quad (7)$$

This reaction was proposed by Nielsen (1979) to represent an important f_{O_2} buffer in peralkaline rocks. In some samples, both reactions took place:

$$Na_3Fe_5Si_8O_{22}(OH)_2 + 4\ FeTiO_3 + 6SiO_2 + 4Na^+ + 2O_2 + 5H_2O \rightarrow 7NaFeSi_2O_6 + Fe_2O_3 + 4Ti^{4+} + 12OH^-. \quad (8)$$

However, some needle-shaped, radially arranged aegirine seems to have precipitated without interaction with, or decomposition of, arfvedsonite or ilmenite. These aggregates may have formed directly from the fluid phase. In some places, they are associated with astrophyllite (Fig. 2h). Similar mineral associations with astrophyllite from other peralkaline granites have been reported by, for example, Marsh (1975), Abdel-Rahman (1992) and Schmitt *et al.* (2000).

T–f_{O_2} *constraints on aegirine formation*

The stability of aegirine in the presence of water is restricted to conditions between the FMQ and HM buffer curves (Bailey, 1969). The occurrence of Ti-free haematite, and relatively Ti-poor aegirine indicates oxidized conditions at or above the HM buffer. The decomposition of arfvedsonite into aegirine, quartz and haematite was reported in the Puklen rocks by Parsons (1972), and in other peralkaline granites by, for example, Boily & Williams-Jones (1994) and Schmitt *et al.* (2000). Reaction (6) represents an f_{O_2} buffer in peralkaline rocks and may be used to estimate the conditions of aegirine formation. Figure 14 shows the T–f_{O_2} dependence of this reaction at 1 kbar using thermodynamic data for aegirine, haematite, quartz and water from Robie & Hemingway (1995). $\Delta_f H^0$ and S^0 for arfvedsonite were estimated using the methods of Robinson & Haas (1983) and Chermak & Rimstidt (1989). The molar volume from Hawthorne (1976) of arfvedsonite (28·17 J/bar) was used. Temperature-dependent fugacity coefficients for water are from Burnham *et al.* (1969). Activities for aegirine, haematite, quartz and water were assumed to be unity. The activity of arfvedsonite varied between 0·1 and 0·15 using a 'mixing on site' model. The uncertainty of these calculations is mainly based on the estimation of $\Delta_f H^0$. It is believed to be in the range of 0·2% (Chermak & Rimstidt, 1989). The grey field around the calculated curves in Fig. 14 marks the uncertainty if an error of ±0·2% for $\Delta_f H^0$(arf) is assumed. The intersection with the HM buffer curve divides this curve into a metastable (high-temperature) and a stable (low-temperature) branch. Assuming a stable formation of aegirine, these intersections should reflect maximum crystallization temperatures of ~260–280°C. If the assumed uncertainty is taken into account, the formation of aegirine took place at temperatures below 450°C.

Popp & Gilbert (1972) showed that the solubility of jadeite in aegirine at constant pressure increases with falling temperature if aegirine coexists with albite and quartz (which is the case for the Puklen aegirines). They investigated the stability of aegirine–jadeite

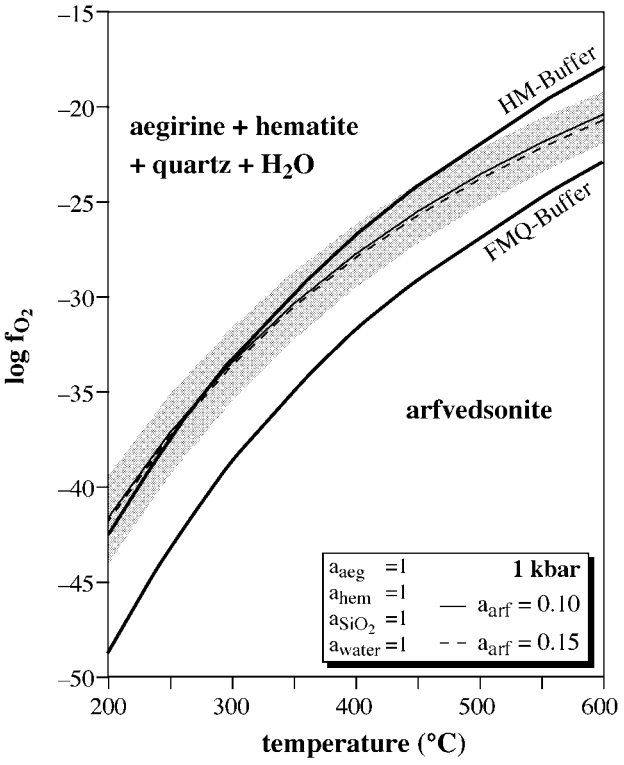

Fig. 14. Log f_{O_2}–T diagram showing the position of reaction (6). The FMQ and HM buffer curves are indicated. The grey field marks the uncertainty if an error of ±0·2 % for $\Delta_f H^0$(arf) is assumed.

solid solutions at low pressures for temperatures between 300° and 600°C. Assuming a pressure of 1 kbar, temperatures below ~350°C are indicated, which is in good agreement with the calculations above.

Whereas Bonin (1986) proposed temperatures of 600–625°C for conversion of arfvedsonite into aegirine + quartz + haematite + H_2O, Boily & Williams-Jones (1994) demonstrated, based on oxygen isotope data, that aegirine formed at significantly lower temperatures, in agreement with our estimate.

RETENTION AND ALTERATION OF PRIMARY ISOTOPE SYSTEMATICS

Oxygen isotope fractionation

In this section, we discuss whether the measured oxygen isotope compositions of minerals represent primary magmatic values or the effects of hydrothermal alteration or re-equilibration during slow cooling.

In syenites, oxygen isotope fractionations between different minerals within the same sample are: $\Delta_{qtz\text{-}aug}$ = +2·6 to +2·8‰; $\Delta_{qtz\text{-}am\ I}$ = +3·5 to +4·2‰; $\Delta_{qtz\text{-}am\ II}$ = +5·1 to +5·6‰. The fractionations between quartz and augite indicate equilibrium at magmatic temperatures of 750–700°C using the fractionation factors of Zheng (1993*a*, 1993*b*). This is in good agreement with the results obtained from feldspar thermometry. The only exception is sample GM1616, with a remarkably large $\Delta_{qtz\text{-}aug}$ of +3·3‰, which is due to the exceptionally low $\delta^{18}O$ value of augite from this sample (+4·7‰). This low value can be explained by the fact that augite in this sample is strongly affected by late-stage peralkaline fluids. From early magmatic augite to later amphibole I and amphibole II, fractionation increases, giving rise to lower apparent equilibrium temperatures (640–570°C and 500–465°C, respectively).

In granophyres, the measured fractionations between quartz and amphibole I (+3·7 and +4·2‰) and between quartz and amphibole II (+5·0 and +5·4‰) are almost identical to those of the syenites, but this value is very small for quartz–augite (+1·0‰) in sample GM1593. This low value and the resulting high calculated equilibrium temperature of >1300°C indicate non-equilibrium conditions for the two minerals in this sample. Because fractionations between quartz, amphibole I and amphibole II show similar values to those in the syenites, it can be concluded either that the augites of sample GM1593 are xenocrysts or that the quartz and amphibole equilibrated with a distinctly different fluid or melt at lower temperatures, whereas the augite did not. Based on their major element and oxygen isotope composition, we assume that these augites are early crystals and were incorporated from the syenites.

In alkali granite and microgranites, quartz–amphibole fractionations vary between +3·6 and +5·3‰, yielding low apparent equilibrium temperatures of 640–480°C. It appears that quartz and amphibole are not in isotopic equilibrium at magmatic temperatures of ~700°C. Possibly, a late closure to oxygen diffusion of quartz caused by low cooling rates may have caused an increase in $\Delta_{qtz\text{-}amph}$. Differences in $\delta^{18}O$ values between late-stage aegirine and quartz are high (+4·6 to +6·1‰) and indicate low apparent equilibrium temperatures of <250°C (Zheng, 1993*a*).

Different effects on the Rb–Sr and the Sm–Nd systems during metasomatism

As mentioned above, the Rb–Sr isotope system has been disturbed and no longer reflects primary magmatic values. Disturbance of the Rb–Sr system is common because Rb and Sr are highly mobile in metasomatic fluids. This has been shown in many whole-rock studies (e.g. Stevenson *et al.*, 1997; Ashwal *et al.*, 2002). The extremely low calculated initial $^{87}Sr/^{86}Sr$ values indicate loss of radiogenic Sr and/or the addition of Rb. Trace element data for augite of

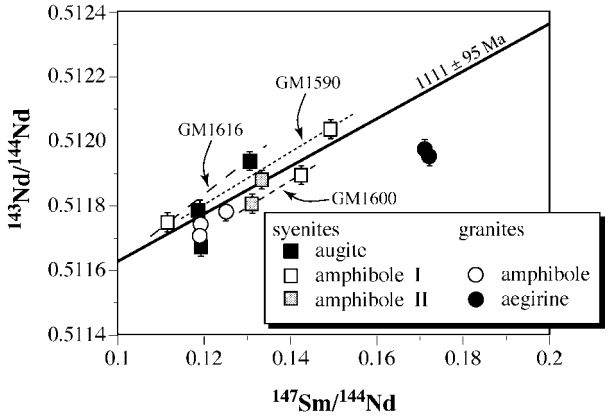

Fig. 15. Sm–Nd isotope diagram for all analysed mineral separates. The line of best fit of 1111 ± 95 Ma was calculated after the method of Brooks *et al.* (1972), neglecting the data for late-stage aegirine separates. Two-point isochrons are shown for syenite samples GM1590, GM1600 and GM1616.

sample GM1616 (Fig. 7) indicate that probably the latter was the case. Additionally, despite the high present-day $^{87}Rb/^{86}Sr$ ratio, a relatively low present-day $^{87}Sr/^{86}Sr$ ratio was measured for the augite of sample GM1616. This indicates that the $^{87}Sr/^{86}Sr$ ratio of the infiltrating late-stage fluid must have been significantly lower than that of the primary magmatic fluid and metasomatism changed both the $^{87}Rb/^{86}Sr$ and $^{87}Sr/^{86}Sr$ ratios of the system.

In contrast to the Rb–Sr system, Sm is positively correlated with Nd and samples with high Sm/Nd and $^{147}Sm/^{144}Nd$ ratios consequently have high present-day $^{143}Nd/^{144}Nd$ ratios (Table 8). These observations suggest that the Sm–Nd system was not as strongly affected by metasomatism as the Rb–Sr system. As shown in Fig. 7c, the concentrations for both Sm and Nd in metasomatized augite increased by a factor of about two compared with unaffected core regions. This effect is relatively small compared with the Rb–Sr system, where the enrichment of Rb and Sr is between 10 and 100. Probably, the similar atomic sizes and resulting physico-chemical characteristics of Sm and Nd are responsible for the similar behaviour of Sm and Nd during late-magmatic processes compared with the drastic differences between Rb and Sr. Therefore, we conclude that the Nd isotopic compositions can be used for geological interpretations.

Figure 15 summarizes the Nd isotopic data in a conventional isochron diagram. The most obvious feature is that the data do not define a single isochron but a trend line at best. The two separates of aegirine from alkali granites show the most pronounced deviation from the general trend. Omitting the aegirine data, a late Gardar age of 1111 ± 95 Ma is obtained. This is in agreement with the assumption that the Puklen rocks intruded penecontemporaneously with the Nunarssuit complex (Pulvertaft, 1961; Finch *et al.*, 2001). The large uncertainty and high MSWD value (mean of squared weighted deviations) of the isochron could result from the relatively low variation in $^{147}Sm/^{144}Nd$ ratios, from analytical errors, from a post-magmatic modification of the Sm–Nd system as mentioned above (e.g. Andersen, 1984) or from heterogeneous initial isotopic compositions of the samples as discussed below. However, in three syenitic samples (GM1590, GM1600 and GM1616), two minerals were analysed and in all three cases the calculated ε_{Nd} values of these separates agree well within error (Table 8). Two-point isochrons defined by these samples agree with the above-mentioned age within error (Fig. 15). This supports the petrological and oxygen isotopic results that suggest an essentially closed-system behaviour for each syenite sample after contamination and during cooling (see below).

MELT SOURCE AND CONTAMINATION

Mineral–melt fractionations allow the calculation of the magma oxygen isotopic compositions directly from measured values of minerals (Taylor & Sheppard, 1986). We used $\Delta_{quartz\text{-}melt}$ and $\Delta_{pyroxene\text{-}melt}$ of Kalamarides (1986), Taylor & Sheppard (1986) and Harris (1995) to calculate $\delta^{18}O_{melt}$ values for the Puklen syenites. For granophyres, only $\Delta_{quartz\text{-}melt}$ was used, as the augite of sample GM1593 is not believed to be in equilibrium with quartz because of unreasonably low $\Delta_{quartz\text{-}augite}$. For the coarse alkali granites and microgranites, only $\Delta_{quartz\text{-}melt}$ was used because aegirine is of hydrothermal origin.

The estimates of $\delta^{18}O_{melt}$ vs wt % SiO_2, showing broadly a negative correlation, are plotted in Fig. 16. Syenites have $\delta^{18}O_{melt}$ values of +5·9 to +6·3‰ and granophyres have slightly lower values (+5·4 and +5·7‰). Coarse alkali granites (+5·1 and +5·3‰) are significantly lower in $\delta^{18}O_{melt}$ than the syenites. If it is considered that $\delta^{18}O_{melt}$ estimates for granites are maxima, as $\Delta_{qtz\text{-}am}$ in the alkali granites (see above) indicates a late closure of quartz to oxygen diffusion, the measured $\delta^{18}O$ values for quartz in granites are likely to be higher than values calculated at the crystallization temperatures of quartz. It is well known that the closure temperature for quartz is, depending on grain size, ~500°C (e.g. Giletti & Yund, 1984; Jenkin *et al.*, 1991). During closed-system cooling, the $\delta^{18}O$ value of quartz will increase relative to other minerals. Therefore, $\delta^{18}O_{melt}$ values for granites are possibly even lower than calculated. Microgranites yielded the lowest $\delta^{18}O_{melt}$ values (+4·7 and +5·2‰).

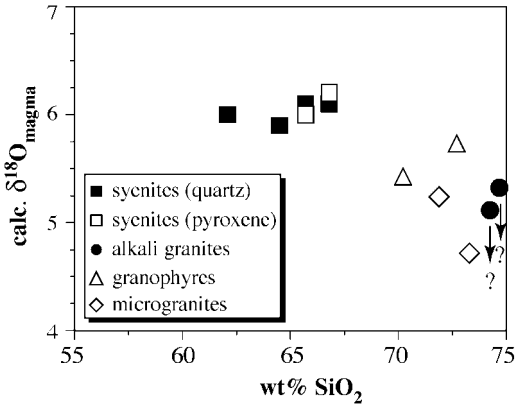

Fig. 16. Calculated oxygen isotopic compositions for the Puklen melts after the methods of Kalamarides (1986), Taylor & Sheppard (1986) and Harris (1995). The homogeneous values for the syenitic parental melt are in contrast to significantly lower and rather inhomogeneous values for the other rock types. The calculated $\delta^{18}O_{melt}$ values for coarse alkali granites are maximum estimates. (See text for further explanation.)

The calculated $\delta^{18}O_{melt}$ value of +5·9 to +6·3‰ for syenites essentially supports a mantle derivation of the parent magma (Kyser, 1986). The analysed mineral separates from syenites span a large range in ε_{Nd} values between –3·8 and –6·4 (Table 8). These differences probably indicate that different magma batches derived from the same source experienced variable amounts of crustal contamination with country rocks during emplacement. Consequently, sample GM1600 ($\varepsilon_{Nd} = -6{\cdot}4$) may represent a strongly contaminated magma, whereas sample GM1616 possibly reflects the least contaminated magma with an ε_{Nd} value of –3·8 for primary augite. The high quartz content of sample GM1600 is therefore believed to be due to a high amount of contamination with silicic country rock in this sample and not due to the effects of fractional crystallization.

The differences in inferred $\delta^{18}O_{melt}$ values between the syenites and the other Puklen rocks cannot be due to closed-system fractionation processes (Kalamarides, 1986; Baker *et al.*, 2000). Moreover, the data obtained during this study indicate at least two isotopically different sources and possibly a mixing between these two. The low $\delta^{18}O_{melt}$ values of the coarse alkali granites and granophyres can be explained only if the magma was derived from a source rock with a low $\delta^{18}O$ value, or contamination with material of low $\delta^{18}O$ has occurred. Three whole-rock $\delta^{18}O$ analyses for basement rocks of the Isortoq area (Fig. 1b) have a mean of +7·8 ± 0·5‰ (R. Halama, unpublished data, 2002). Consequently, the upper granitic crust of the Gardar Province is not a significant contaminant for the Puklen granites. Other contaminants or sources with low $\delta^{18}O$—for example, lower-crustal rocks (Valley, 1986) or sources that were already altered by meteoric fluids before melting (Harris & Ashwal, 2002)—are necessary to explain the oxygen isotopic differences between the syenites and the other Puklen rocks.

EFFECTS OF LATE-STAGE PROCESSES ON OXYGEN ISOTOPE COMPOSITIONS

Late-stage minerals from the syenites (amphibole II) and alkali granites (aegirine) have much lower $\delta^{18}O$ values than the primary magmatic minerals. Petrological criteria indicate that amphibole II in the syenites formed at temperatures below ~550°C and aegirine at even lower temperatures, possibly <300°C (see above). Principally, two contrasting explanations for these low $\delta^{18}O$ values are possible: (1) the late-stage minerals formed in the presence of a low-$\delta^{18}O$ fluid; (2) the low values reflect increasing fractionation at lower temperatures between minerals open to oxygen exchange.

To evaluate these two possibilities, changes in the $\delta^{18}O$ values of the minerals and the coexisting fluid phase during cooling were modelled for both rock types. For the calculation of the closed-system evolution in the syenites, the following assumptions were made:

(1) quartz, augite and amphibole I were in isotopic equilibrium at magmatic temperatures of 700–800°C. Using the fractionation factors of Bottinga & Javoy (1975) and Zheng (1993*a*), the calculated feldspar composition at the magmatic stage would have been between +6·5 and +7·5‰.

(2) The calculated oxygen isotope composition of coexisting water (which is used as an approximation for the water-dominated fluid phase in amphibole II-bearing syenites) at these temperatures ranges from +6·3 to +7·5‰ based on fractionation factors of Zheng (1993*a*, 1993*b*).

(3) During cooling and amphibole II formation, oxygen exchange was possible only between amphibole II, feldspar and the coexisting fluid phase. Quartz, augite and amphibole I closed to oxygen diffusion at temperatures below 500°C (Giletti *et al.*, 1978; Giletti & Yund, 1984; Farver & Giletti, 1985; Farver, 1989).

(4) Fluid/rock ratios are small enough that the fluid does not represent an inexhaustible reservoir that would retain a constant oxygen isotopic composition, independent of temperature or minerals it is in equilibrium with.

(5) As a simplification, the oxygen contents of amphibole and feldspar are assumed to be equal.

Feldspar modally dominates over amphibole. From thin sections, the modal ratio between feldspar and amphibole II was estimated to be about 95:5.

Given the above assumptions, the $\delta^{18}O$ value of the system open to exchange at any temperature is defined by

$$\delta^{18}O_{system} = 0{\cdot}95\delta^{18}O_{fsp} + 0{\cdot}05\delta^{18}O_{am}. \quad (9)$$

Using the temperature-dependent fractionation factors of Bottinga & Javoy (1975), $\delta^{18}O_{fsp}$ is given by

$$\delta^{18}O_{fsp}(\text{at a given temperature}) = e\left(\frac{1000\ln\alpha_{fsp-am}}{1000}\right)(\delta^{18}O_{am} + 1000) - 1000. \quad (10)$$

Solving equations (9) and (10) simultaneously allows the calculation of $\delta^{18}O_{am}$ and $\delta^{18}O_{fsp}$. Figure 17 illustrates the results of these calculations. Calculated and measured $\delta^{18}O$ values for amphibole II are equal at temperatures of ~400°C. This fits well with the petrological results. Hence, the low $\delta^{18}O$ values measured for amphibole II in syenites can be explained by a closed-system cooling model. Feldspar should have an oxygen isotope composition of +6·5 to +7·5‰ at a temperature of ~400°C, which is in agreement with a published $\delta^{18}O$ value of about +6·5‰ for fresh feldspar from the Puklen complex (Sheppard, 1986).

However, measured values of altered perthitic feldspar are much lower, between about +3 and +4‰, indicating a late hydrothermal alteration in the presence of low-$\delta^{18}O$ fluids. As the dominant mineral in the syenites is alkali feldspar, this mineral dominates the whole-rock oxygen isotopic composition. A rough estimate, assuming 15 vol. % quartz (with constant values of about +8‰), ~15% mafic minerals (average of about +5‰) and ~70 vol. % feldspar indicates that the inhomogeneous whole-rock $\delta^{18}O$ values measured for syenites (+4·8 to +6·9‰) must largely be due to variation of the oxygen isotope composition of the alkali feldspar. Calculated $\delta^{18}O$ values of the altered feldspar thus vary between about +2·8 and +5·0‰. This is in agreement with two measured values of altered feldspar (+3·5 and +3·9‰, Table 7). Whether the $\delta^{18}O$ value of a rock (mineral) increases or decreases during fluid–rock interaction is a function of temperature of alteration, the $\delta^{18}O$ value of the fluid, and of the fluid–rock ratio. At temperatures below ~100°C it is possible that the whole-rock $\delta^{18}O$ value actually increases even if fluids with very low $\delta^{18}O$ values (−10‰ or lower) are involved, simply because the mineral–water O-isotope fractionation factors are very high at these temperatures. However, at higher temperatures this is not the case, as mineral–water fractionation factors decrease with rising temperatures. It is therefore suggested that the heterogeneity of whole-rock $\delta^{18}O$ values is mainly caused by alteration of feldspars by low-$\delta^{18}O$ fluids, probably dominated by meteoric water at temperatures in excess of 100°C. Such alteration has been described from a number of plutonic rocks (e.g. Criss & Taylor, 1986; Lutz *et al.*, 1988).

Applying a closed-system model similar to that described above to the alkali granites for possible feldspar–aegirine exchange, the low $\delta^{18}O$ values of aegirine cannot be explained. If a closed system is

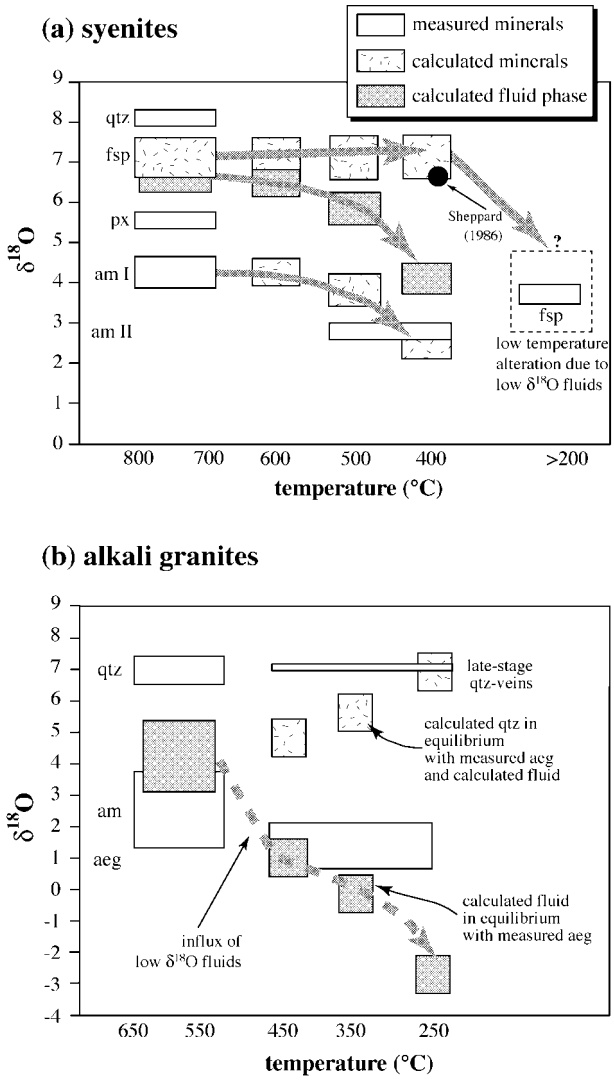

Fig. 17. (a) Variation of $\delta^{18}O$ vs temperature (°C) for the closed-system model for the syenites, illustrating the oxygen isotope evolution of individual minerals and the coexisting fluid phase during cooling. Modelled values are compared with measured data. •, published $\delta^{18}O$ value for fresh feldspar from the Puklen complex (Sheppard, 1986). (b) An influx of the low-$\delta^{18}O$ fluids during late-stage evolution of granites may explain the low $\delta^{18}O$ values of aegirine. (See text for further explanation.)

assumed, the calculated $\delta^{18}O$ values of aegirine are much higher than the measured values. Thus, an influx of low-$\delta^{18}O$ fluids is necessary to explain the isotopic compositions of late-stage aegirine in alkali granites (Fig. 17b). The measured aegirines are in oxygen isotopic equilibrium with late-stage quartz veins at temperatures of ~250°C, which is in good agreement with the petrological results for aegirine formation. The calculated fluid oxygen isotopic composition at these low temperatures is about –3‰, which is more than 7‰ lower than the late-stage, closed-system fluid modelled to be in equilibrium with the syenites. This low-$\delta^{18}O$ fluid could be of meteoric origin. The inferred palaeolatitude for South Greenland during late Gardar times is 30–60°N (Piper, 1992). By comparison with the present-day distribution of isotopic compositions of meteoric waters (e.g. Rozanski *et al.*, 1993), it is likely that values for the local meteoric waters were even lower than our estimate of −3‰. The chemical and isotopic composition of this meteoric fluid may well have been buffered by interaction with the country rocks. During this process it may have also picked up significant quantities of Nd or at least changed its Nd-isotopic composition significantly, resulting in the remarkably low ε_{Nd} values for aegirines. Additionally, this meteoric fluid may also be responsible for the inferred low-temperature alteration of alkali feldspar in the syenites and alkali granites. Although not strictly required, it is also possible that such a fluid has contributed to the decrease of the $\delta^{18}O$ values of amphibole II, a possibility that cannot be excluded on the basis of the present data.

SUMMARY AND CONCLUSIONS

In the alkaline to peralkaline rocks of the Puklen complex two phase assemblages can be distinguished: a primary magmatic and a secondary late- to post-magmatic assemblage. The primary magmatic assemblage in the syenites consists of alkfsp ± qtz + aug ± ol + Fe–Ti oxides and interstitial Na–Ca amphibole. Solvus thermometry of early ternary feldspar phenocrysts indicates minimum crystallization temperatures of ~950–750°C. Oxygen fugacity during this stage was low and ranged from 0·8 to 2·3 log units below the FMQ buffer. Mineral- and whole-rock geochemical data suggest that fractional crystallization of feldspar, olivine, augite, magnetite–ilmenite and apatite from a silica-undersaturated parental magma led to an increase of silica activity from ~0·7 in quartz-free samples towards unity in quartz-bearing ones. The magmatic assemblage in the granites (alkfsp + qtz + am + ilm) crystallized at temperatures >750°C and redox conditions around the FMQ buffer.

A number of processes including fractional crystallization, assimilation of country rocks, post-magmatic alteration and sub-solidus re-equilibration played a significant role in the complex geochemical and isotopic evolution of the Puklen rocks. The O, Sr and Nd isotopic data presented here for the Puklen complex can be used to distinguish between magmatic and post-magmatic processes. This is particularly caused by the fact that the three isotope systems investigated here (O, Rb/Sr, Sm/Nd) are affected to variable degrees during late-stage metasomatism and alteration. Isotopic compositions of different minerals from the same sample indicate a multi-source genesis for the Puklen rocks. Whole-rock analyses in similar cases would be inadequate and lead to complex results and incorrect geological interpretations. Even mineral separates may be problematic if adequate conclusions on magma genesis and late-stage history are desired, as some of the processes mentioned above may overlap each other.

Oxygen isotope compositions indicate that the magmas parental to the syenitic melts of the Puklen complex are compatible with derivation from a mantle source. During ascent of the syenite magmas, variable degrees of contamination with upper-crustal material occurred, which is shown by the large range of ε_{Nd} values in the syenites. In contrast, the oxygen isotopic compositions of the primary minerals and estimated magma compositions are homogeneous (Figs 9 and 16). This may be a consequence of mass balance considerations: as oxygen is a major constituent of silicate rocks, a large contrast in oxygen isotopic composition between primary melt and contaminant is needed to produce significant differences in oxygen isotopic composition. The similar oxygen isotopic composition and the very different Nd isotope characteristics of the granitic upper crust of the Gardar Province fit well with a model in which the Puklen syenites are explained by variable amounts of contamination of a mantle-derived melt by granitic upper crust.

Calculated $\delta^{18}O_{melt}$ values for the alkali granites are significantly lower than those of the syenites (Figs 9 and 18). These low $\delta^{18}O$ values are believed to be a source feature and not an effect of low-temperature oxygen diffusion. However, the ε_{Nd} values for two separates of magmatic amphibole from the alkali granites fall well within the range of ε_{Nd} values from the syenites. Based on the Nd isotopic data, a common source for the syenites and alkali granites may be possible, but the low oxygen isotopic composition of the granites compared with the syenites requires a different contaminant or source with low $\delta^{18}O$ composition, which was not involved in the genesis of the syenites.

Late-stage fluids, which were retained by the syenites, caused the replacement of the primary assemblage by secondary silicates: augite was replaced by

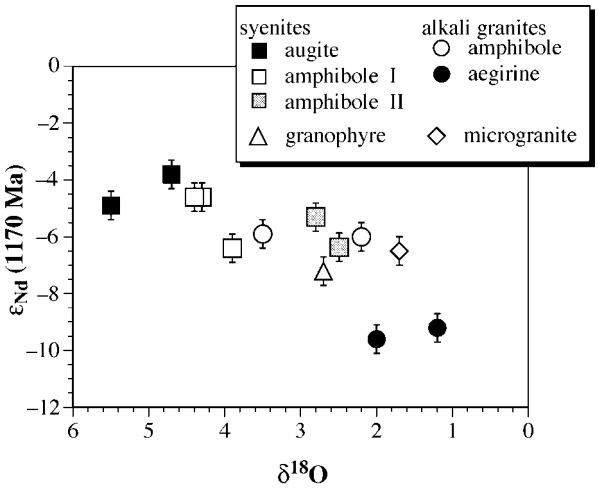

Fig. 18. Correlation diagram of neodymium and oxygen isotopic composition for mineral separates from the Puklen complex.

aegirine–augite, aenigmatite formed at the expense of ilmenite and, as a result of the release of Ca during this process, secondary autometasomatic minerals such as ferro-actinolite, carbonates, hydroandradite and titanite formed. The formation of these secondary Ca-minerals took place over a wide temperature range between about 700° and 300°C. During this cooling, oxygen fugacity rose in most samples to values around the FMQ buffer. It is remarkable that the latest minerals in the syenites are not of a typical peralkaline composition, but are Ca-rich like the primary assemblage. The restriction to the syenites and their absence in the granites implies either a short transport capacity of the fluid phase for these elements or that late-stage autometasomatism in syenites and granites worked differently. Oxygen and neodymium isotope data for these secondary Ca phases indicate that the syenites generally experienced closed-system behaviour during cooling only. A few syenitic samples (GM1611, GM1615 and GM1616) reflect f_{O_2} conditions and temperatures similar to those for the granites. This may indicate that fluids from the granites influenced these samples, as they were collected close to the granite body.

The late-stage formation of aegirine at the expense of arfvedsonite in the granites is shown to be a low-temperature process, which took place at conditions around the HM buffer at temperatures possibly around 300°C. Thus, the granites became more oxidized than the syenites, which possibly implies a different fluid source for the granites. The large oxygen and neodymium isotopic differences between primary amphibole and late-stage aegirine in the granites indicate that the source of the aegirine-forming fluids was isotopically different from that which formed the primary amphiboles. A major influx of a second, meteoric fluid, with low oxygen and neodymium isotope composition, was probably responsible for this. The widespread alteration of feldspar in all rock types of the Puklen complex, which is reflected in the low ^{18}O isotopic composition of the whole rocks, may correlate with this latest meteoric fluid circulation.

ACKNOWLEDGEMENTS

LA–ICP-MS measurements were carried out at the Large Scale Geochemical Facility supported by the European Community–Access to Research Infrastructure action of the Improving Human Potential Programme, contract HPRI-CT-1999-00008 awarded to Professor B. J. Wood (University of Bristol), which is gratefully acknowledged. Bruce Paterson provided invaluable help during these measurements. M. Westphal is thanked for his help during microprobe measurements, Elmar Reitter for his careful help during Sr and Nd isotope measurements, Gaby Stoschek for her help with sample preparation for mass spectrometry and oxygen isotope analysis, and Jasmin Köhler for patient hand picking of mineral separates. Thomas Wenzel helped to improve an earlier version of this manuscript. Extremely thorough reviews and constructive comments by D. Baker, C. Harris, I. Parsons, R. Trumbull and M. Wilson (editor) improved the quality of this work substantially. Financial support for this work was provided by the Deutsche Forschungsgemeinschaft (grant Ma-2135/1-2).

REFERENCES

Abdel-Rahman, A. M. (1992). Mineral chemistry and paragenesis of astrophyllite from Egypt. *Mineralogical Magazine* **56**, 17–26.

Andersen, D. J., Lindsley, D. H. & Davidson, P. M. (1993). QUILF: a PASCAL program to assess equilibria among Fe–Mg–Mn–Ti oxides, pyroxenes, olivine, and quartz. *Computers and Geosciences* **19**, 1333–1350.

Andersen, T. (1984). Secondary processes in carbonatites: petrology of 'rodberg' (hematite–calcite–dolomite carbonatite) in the Fen central complex, Telemark (South Norway). *Lithos* **17**, 227–245.

Anovitz, L. M. & Essene, E. J. (1987). Phase equilibria in the system $CaCO_3$–$MgCO_3$–$FeCO_3$. *Journal of Petrology* **28**, 389–414.

Armstrong, J. T. (1991). Quantitative elemental analysis of individual microparticles with electron beam instruments. In: Heinrich, K. F. J. & Newbury, D. E. (eds) *Electron Probe Quantitation*. New York: Plenum, pp. 261–315.

Ashwal, L. D., Demaiffe, D. & Torsvik, T. H. (2002). Petrogenesis of Neoproterozoic granitoids and related rocks from the Seychelles: the case for an Andean-type arc origin. *Journal of Petrology* **43**, 45–83.

Bailey, D. K. (1969). The stability of acmite in the presence of H_2O. *American Journal of Science* **267-A**, 1–16.

Bailey, J. C., Bohse, H., Gwodzdz, R. & Rose-Hansen, J. (1993). Li in minerals from the Ilímaussaq alkaline intrusion, South Greenland. *Bulletin of the Geological Society of Denmark* **40**, 288–299.

Baker, J. A., MacPherson, C. G., Menzies, M. A., Thirlwall, M. F., Al-Kadasi, M. & Mattey, D. P. (2000). Resolving crustal and mantle contributions to continental flood volcanism, Yemen; constraints from mineral oxygen isotope data. *Journal of Petrology* **41**, 1805–1820.

Bea, F., Arzamastsev, A., Montero, P. & Arzamastseva, L. (2001). Anomalous alkaline rocks of Soustov, Kola: evidence of mantle-derived metasomatic fluids affecting crustal materials. *Contributions to Mineralogy and Petrology* **140**, 554–566.

Berman, R. (1988). Internally consistant thermodynamic data for minerals in the system Na_2O–K_2O–CaO–MgO–FeO–Fe_2O_3–Al_2O_3–SiO_2–TiO_2–H_2O–CO_2. *Journal of Petrology* **29**, 445–522.

Berman, R. G., Brown, T. H. & Perkins, E. H. (1987). Geo-Calc; software for calculation and display of *P–T–X* phase diagrams. *American Mineralogist* **72**, 861–862.

Birkett, T. C., Trzcienski, W. E. & Stirling, J. A. R. (1996). Occurrence and compositions of some Ti-bearing minerals in the Strange Lake Intrusive Complex, Quebec–Labrador boundary. *Canadian Mineralogist* **34**, 779–801.

Boily, M. & Williams-Jones, A. E. (1994). The role of magmatic and hydrothermal processes in the chemical evolution of the Strange Lake plutonic complex, Quebec–Labrador. *Contributions to Mineralogy and Petrology* **118**, 33–47.

Bonin, B. (1986). *Ring Complex Granites and Anorogenic Magmatism*. New York: Elsevier, 188 pp.

Bottinga, Y. & Javoy, M. (1975). Oxygen isotope partitioning among the minerals in igneous and metamorphic rocks. *Reviews of Geophysics and Space Physics* **13**, 401–418.

Brooks, C., Hart, S. R. & Wendt, I. (1972). Realistic use of two-error regression treatments as applied to rubidium–strontium data. *Reviews in Geophysics and Space Physics* **10**, 551–577.

Buddington, A. F. & Lindsley, D. H. (1964). Iron–titanium oxide minerals and synthetic equivalents. *Journal of Petrology* **5**, 310–357.

Burnham, C. W., Holloway, J. R. & Davis, N. F. (1969). Thermodynamic Properties of Water to 1000°C and 10 000 bars. *Geological Society of America, Special Papers* **132**.

Caroff, M., Maury, R. C., Leterrier, J., Joron, J. L., Cotten, J. & Guille, G. (1993). Trace element behavior in the alkali basalt–comenditic trachyte series from Mururoa atoll, French Polynesia. *Lithos* **30**, 1–22.

Chakhmouradian, A. R. & Mitchell, R. H. (2002). The mineralogy of Ba- and Zr-rich alkaline pegmatites from Gordon Butte, Crazy Mountains (Montana, USA): comparisons between potassic and sodic agpaitic pegmatites. *Contributions to Mineralogy and Petrology* **143**, 93–114.

Chermak, J. A. & Rimstidt, J. D. (1989). Estimating the thermodynamic properties (ΔG_f^0 and ΔH_f^0) of silicate minerals at 298 K from the sum of polyhedral contributions. *American Mineralogist* **74**, 1023–1031.

Clayton, R. N. & Mayeda, T. K. (1963). The use of bromine pentafluoride in the extraction of oxygen from oxides and silicates for isotope analysis. *Geochimica et Cosmochimica Acta* **27**, 43–52.

Cosca, M. A., Moecher, D. P. & Essene, E. J. (1986). Activity–composition relations for the join grossular–andradite and application to calc-silicate assemblages. *Geological Society of America, Abstracts with Programs* **18**, 572.

Coulson, I. M. (1997). Post-magmatic alteration in eudialyte from the North Qoroq centre, South Greenland. *Mineralogical Magazine* **61**, 99–109.

Criss, R. E. & Taylor, H. P., Jr (1986). Meteoric–hydrothermal systems. In: Valley, J. W., Taylor, H. P., Jr & O'Neil, J. R. (eds) *Stable Isotopes. Mineralogical Society of America, Reviews in Mineralogy* **16**, 373–422.

Davies, G. R. & Macdonald, R. (1987). Crustal influences in the petrogenesis of the Naivasha basalt–comendite complex: combined trace element and Sr–Nd–Pb isotope constraints. *Journal of Petrology* **28**, 1009–1031.

Dunworth, E. A. & Bell, K. (2001). The Turiy massif, Kola peninsula, Russia: isotopic and geochemical evidence for multi-source evolution. *Journal of Petrology* **42**, 377–405.

Edgar, A. D. & Parker, L. M. (1974). Comparison of melting relationships of some plutonic and volcanic peralkaline undersaturated rocks. *Lithos* **7**, 263–273.

Elkins, L. T. & Grove, T. L. (1990). Ternary feldspar experiments and thermodynamic models. *American Mineralogist* **75**, 544–559.

Emeleus, C. H. & Upton, B. G. J. (1976). The Gardar period in southern Greenland. In: Escher, A. & Watt, W. S. (eds) *Geology of Greenland*. Copenhagen: Geological Survey of Greenland, pp. 152–181.

Escher, A. & Watt, W. S. (eds) (1976). *Geology of Greenland*. Copenhagen: Geological Survey of Greenland, 603 pp.

Farver, J. R. (1989). Oxygen self-diffusion in diopside with application to cooling rate determinations. *Earth and Planetary Science Letters* **92**, 386–396.

Farver, J. R. & Giletti, B. J. (1985). Oxygen diffusion in amphiboles. *Geochimica et Cosmochimica Acta* **49**, 1403–1411.

Finch, A. A., Parsons, I. & Mingard, S. C. (1995). Biotites as indicators of fluorine fugacities in late-stage magmatic fluids: the Gardar Province in South Greenland. *Journal of Petrology* **36**, 1701–1728.

Finch, A. A., Mansfeld, J. & Andersen, T. (2001). U–Pb radiometric age of Nunarsuit pegmatite, Greenland: constraints on the timing of Gardar magmatism. *Bulletin of the Geological Society of Denmark* **48**, 1–7.

Foland, K. A., Landoll, J. D., Henderson, C. M. B. & Jiangfeng, C. (1993). Formation of cogenetic quartz and nepheline syenites. *Geochimica et Cosmochimica Acta* **57**, 697–704.

Frisch, W. & Abdel-Rahman, A. M. (1999). Petrogenesis of the Wadi Dib alkaline ring complex, Eastern Desert of Egypt. *Mineralogy and Petrology* **65**, 249–275.

Frost, B. R. & Lindsley, D. H. (1992). Equilibria among Fe–Ti-oxides, pyroxenes, olivine, and quartz: Part II. Application. *American Mineralogist* **77**, 1004–1020.

Ghiorso, M. S. & Evans, B. W. (2002). Thermodynamics of the amphiboles: Ca–Mg–Fe^{2+} quadrilateral. *American Mineralogist* **87**, 79–98.

Gilbert, M. C. & Briggs, D. F. (1974). Comparison of the stabilities of OH- and F-potassic richterites; a preliminary report. *EOS Transactions, American Geophysical Union* **55**, 480–481.

Giletti, B. J. & Yund, R. A. (1984). Oxygen diffusion in quartz. *Journal of Geophysical Research* **89**, 4039–4046.

Giletti, B. J., Semet, M. P. & Yund, R. A. (1978). Studies in diffusion—III. Oxygen in feldspars: an ion microprobe determination. *Geochimica et Cosmochimica Acta* **42**, 45–57.

Goldsmith, J. R., Graf, D. L., Witters, J. & Northtrop, D. A. (1962). Studies in the system $CaCO_3$–$MgCO_3$–$FeCO_3$: 1. Phase relations; 2. A method for major-element spectrochemical analysis; 3. Compositions of some ferroan dolomites. *Journal of Geology* **70**, 659–688.

Goldstein, S. L., O'Nions, R. K. & Hamilton, P. J. (1984). A Sm–Nd isotopic study of the atmospheric dust and particulates from major river systems. *Earth and Planetary Science Letters* **70**, 221–236.

Grapes, R., Yagi, K. & Okumura, K. (1979). Aenigmatite, sodic pyroxene, arfvedsonite and associated minerals in syenites from Morotu, Sakhalin. *Contributions to Mineralogy and Petrology* **69**, 97–103.

Halama, R., Waight, T. & Markl, G. (2002). Geochemical and isotopic zoning patterns of plagioclase megacrysts in gabbroic dykes from the Gardar Province, South Greenland: implications for crystallization processes in anorthositic magmas. *Contributions to Mineralogy and Petrology* **144**, 109–127.

Harris, C. (1983). The petrology of lavas and associated plutonic inclusions of Ascension island. *Journal of Petrology* **24**, 424–470.

Harris, C. (1995). Oxygen isotope geochemistry of the Mesozoic anorogenic complexes of Damaraland, northwest Namibia: evidence for crustal contamination and its effects on silica saturation. *Contributions to Mineralogy and Petrology* **122**, 308–321.

Harris, C. & Ashwal, L. D. (2002). The origin of low $\delta^{18}O$ granites and related rocks from the Seychelles. *Contributions to Mineralogy and Petrology* **143**, 366–376.

Harry, W. T. & Pulvertaft, C. T. R. (1963). The Nunarssuit Intrusive Complex, South Greenland. *Bulletin Grønlands Geologiske Undersøgelse* **36**, 136 pp.

Hawthorne, F. C. (1976). The crystal chemistry of the amphiboles; V, The structure and chemistry of arfvedsonite. *Canadian Mineralogist* **14**, 346–356.

Hawthorne, F. C., Ungaretti, L., Oberti, R. & Bottazzi, P. (1993). Li: an important component in igneous alkali amphiboles. *American Mineralogist* **78**, 733–745.

Hawthorne, F. C., Ungaretti, L., Oberti, R. & Cannillo, E. (1994). The mechanisms of [6]Li incorporation in amphiboles. *American Mineralogist* **79**, 443–451.

Hawthorne, F. C., Oberti, R., Cannillo, E. & Ottolini, L. (2001). Li-bearing arfvedsonitic amphiboles from the Strange Lake peralkaline granite, Quebec. *Canadian Mineralogist* **39**, 1161–1170.

Heaman, L. M. & Machado, N. (1992). Timing and origin of midcontinent rift alkaline magmatism, North America: evidence from the Coldwell Complex. *Contributions to Mineralogy and Petrology* **110**, 289–303.

Hellner, E. & Schürmann, K. (1966). Stability of metamorphic amphiboles: the tremolite–ferroactinolite series. *Journal of Geology* **74**, 323–331.

Holland, T. J. B. (1990). Activities of components in omphacitic solid solutions; an application of Landau theory of mixtures. *Contributions to Mineralogy and Petrology* **105**, 446–453.

Ike, E. C. (1985). Postmagmatic arfvedsonite–aenigmatite paragenesis in the ring-dyke of the Burra Centre, Ningi-Burra complex, Nigeria. *Journal of African Earth Sciences* **3**, 101–105.

Jacobson, S. B. & Wasserburg, G. J. (1980). Sm–Nd isotopic evolution of chondrites. *Earth and Planetary Science Letters* **50**, 139–155.

Jenkin, G. R. T., Linklater, C. & Fallick, A. E. (1991). Modeling of mineral $\delta^{18}O$ values in an igneous aureole: closed-system model predicts apparent open-system $\delta^{18}O$ values. *Geology* **19**, 1185–1188.

Kalamarides, R. I. (1986). High-temperature oxygen isotope fractionation among the phases of Kiglapait intrusion, Labrador, Canada. *Chemical Geology* **58**, 303–310.

Kogarko, L. N. & Romanchev, B. P. (1977). Temperature, pressure, redox conditions, and mineral equilibria in agpaitic nepheline syenites and apatite–nepheline rocks. *Geochemistry International* **14**, 113–128.

Kogarko, L. N. & Romanchev, B. P. (1982). Phase equilibria in alkaline melts. *International Geology Review* **25**, 534–546.

Konnerup-Madsen, J. & Rose-Hansen, J. (1984). Composition and significance of fluid inclusions in the Ilímaussaq peralkaline granite, South Greenland. *Bulletin de Minéralogie* **107**, 317–326.

Kramm, U. & Kogarko, L. N. (1994). Nd and Sr isotope signatures of the Khibina and Lovozero agpaitic centres, Kola Province, Russia. *Lithos* **32**, 225–242.

Kresten, P. (1988). The chemistry of fenitization, examples from Fen, Norway. *Chemical Geology* **68**, 329–349.

Kunzendorf, H., Nyegaard, P. & Nielsen, B. L. (1982). Distribution of Characteristic Elements in the Radioactive Rocks of the Northern Part of Kvanefjeld, Ilimaussaq Intrusion, South Greenland. *Rapport Grønlands Geologiske Undersøgelse* **109**, 32 pp.

Kunzmann, T. (1999). The aenigmatite–rhönite mineral group. *European Journal of Mineralogy* **11**, 743–756.

Kyser, T.K. (1986). Stable isotope variations in the mantle. In: Valley, J.W., Taylor, H.P.Jr & O'Neil, J.R. (eds). *Stable Isotopes. Reviews in Mineralogy. Mineralogical Society of America* **16**, 141–161.

Larsen, L. M. (1976). Clinopyroxenes and coexisting mafic minerals from the alkaline Ilímaussaq intrusion, South Greenland. *Journal of Petrology* **17**, 258–290.

Larsen, L. M. (1977). Aenigmatites from the Ilímaussaq intrusion, South Greenland: chemistry and petrological implications. *Lithos* **10**, 257–270.

Larsen, L. M. & Sørensen, H. (1987). The Ilímaussaq intrusion—progressive crystallization and formation of layering in an agpaitic magma. In: Fitton, J. G. & Upton, B. G. J. (eds) *Alkaline Igneous Rocks. Geological Society, London, Special Publications* **30**, 473–488.

Leake, B. E., Wooley, A. R., Arps, C. E. S., Birch, W. D., Gilbert, M. C., Grice, J. D., *et al.* (1997). Nomenclature of amphiboles: Report of the Subcommittee on Amphiboles of the International Mineralogical Association, Commission on New Minerals and Mineral Names. *American Mineralogist* **82**, 295–321.

Liebermann, J. & Petrakakis, K. (1990). TWEEQU thermobarometry, analysis of uncertainties and applications to granulites from western Alaska. *Canadian Mineralogist* **29**, 857–887.

Lindsley, D. H. (1983). Pyroxene thermometry. *American Mineralogist* **68**, 477–493.

Lindsley, D. H. & Frost, B. R. (1992). Equilibria among Fe–Ti-oxides, pyroxenes, olivine, and quartz: Part I. Theory. *American Mineralogist* **77**, 987–1003.

Lugmair, G. W. & Marti, K. (1978). Lunar initial $^{143}Nd/^{144}Nd$: differential evolution of the lunar crust and mantle. *Earth and Planetary Science Letters* **39**, 349–357.

Lutz, T. M., Foland, K. A., Faul, H. & Srogi, L. A. (1988). The strontium and oxygen isotopic record of hydrothermal alteration of syenites from the Abu Khruq complex, Egypt. *Contributions to Mineralogy and Petrology* **98**, 212–223.

Markl, G. (2001). Stability of Na–Be minerals in late-magmatic fluids of the Ilímaussaq alkaline complex, South Greenland. *Geology of Greenland Survey Bulletin* **190**, 145–158.

Markl, G. & Baumgartner, L. (2002). pH changes in peralkaline late magmatic fluids. *Contributions to Mineralogy and Petrology* **144**, 331–346.

Markl, G., Marks, M., Schwinn, G. & Sommer, H. (2001). Phase equilibrium constraints on intensive crystallization parameters of the Ilímaussaq Complex, South Greenland. *Journal of Petrology* **42**, 2231–2258.

Marks, M. & Markl, G. (2001). Fractionation and assimilation processes in the alkaline augite syenite unit of the Ilímaussaq Intrusion, South Greenland, as deduced from phase equilibria. *Journal of Petrology* **42**, 1947–1969.

Marsh, J. S. (1975). Aenigmatite stability in silica-undersaturated rocks. *Contributions to Mineralogy and Petrology* **50**, 135–144.

Mingram, B., Trumbull, R. B., Littman, S. & Gerstenberger, H. (2000). A petrogenetic study of anorogenic felsic magmatism in the Cretaceous Paresis ring complex, Namibia: evidence for mixing of crust and mantle-derived components. *Lithos* **54**, 1–22.

Morogan, V. (1989). Mass transfer and REE mobility during fenitization at Alnö, Sweden. *Contributions to Mineralogy and Petrology* **103**, 25–34.

Nicholls, J. & Carmichael, I. S. E. (1969). Peralkaline acid liquids: a petrological study. *Contributions to Mineralogy and Petrology* **20**, 268–294.

Nielsen, T. F. D. (1979). The occurrence and formation of Ti-aegirines in peralkaline syenites; an example from the Tertiary ultramafic alkaline Gardiner complex, East Greenland. *Contributions to Mineralogy and Petrology* **69**, 235–244.

Parsons, I. (1972). Petrology of the Puklen Syenite–Alkali Granite Complex, Nunarssuit, South Greenland. *Meddelelser om Grønland* **195**, 73 pp.

Parsons, I. (1979). The Klokken gabbro–syenite complex, South Greenland: cryptic variation and origin of inversely graded layering. *Journal of Petrology* **20**, 653–694.

Parsons, I., Mason, R. A., Becker, S. M. & Finch, A. A. (1991). Biotite equilibria and fluid circulation in the Klokken Intrusion. *Journal of Petrology* **32**, 1299–1333.

Perry, F.V., Baldridge, W.S. & DePaolo, D.J. (1987). Role of asthenosphere and lithosphere in the genesis of late Cenozoic basaltic rocks from the Rio Grande rift and adjacent regions of the Southwestern United States. *Journal of Geophysical Research* **92**, 9193–9213.

Piotrowski, J. M. & Edgar, A. D. (1970). Melting Relations of Undersaturated Alkaline Rocks from South Greenland. *Meddelelser om Grønland* **181**(9), 62 pp.

Piper, J. D. A. (1992). The palaeomagnetism of major (Middle Proterozoic) igneous complexes, South Greenland and the Gardar apparent polar wander track. *Precambrian Research* **54**, 153–172.

Popp, R. K. & Gilbert, M. C. (1972). Stability of acmite–jadeite pyroxenes at low pressure. *American Mineralogist* **57**, 1210–1231.

Poulsen, V. (1964). The Sandstones of the Precambrian Eriksfjord Formation in South Greenland. *Rapport Grønlands Geologiske Undersøgelse* **2**, 16 pp.

Powell, M. (1978). The crystallisation history of the Igdlerfigssalik nepheline syenite intrusion, Greenland. *Lithos* **11**, 99–120.

Pulvertaft, T. C. R. (1961). The Puklen intrusion, Nunarssuit, SW Greenland. *Meddelelser om Grønland* **123**(6), 35–49.

Robie, R. A. & Hemingway, B. S. (1995). Thermodynamic Properties of Minerals and Related Substances at 298·15 K and 1 bar (10^5 Pascals) Pressure and at Higher Temperatures. *US Geological Survey Bulletin* **2131**, 461 pp.

Robinson, G. R., Jr & Haas, J. L., Jr (1983). Heat capacity, relative enthalpy, and calorimetric entropy of silicate minerals: an empirical method of prediction. *American Mineralogist* **68**, 541–553.

Rock, N. M. S. (1976). Fenitisation around the Monchique alkaline complex, Portugal. *Lithos* **9**, 263–279.

Roddick, J. C., Sullivan, R. W. & Dudas, F. Ö. (1992). Precise calibration of Nd tracer isotopic composition for Sm–Nd studies. *Chemical Geology* **97**, 1–8.

Rozanski, K., Araguás-Araguás, L. & Gonfiantini, R. (1993). Isotopic patterns in modern global precipitation. In: Swart, P. K., Lohmann, K. C., McKenzie, J. A. & Savin, S. (eds) *Climate Change in Continental Isotopic Records. Geophysical Monograph, American Geophysical Union* **78**, 1–36.

Rumble, D. & Hoering, T. C. (1994). Analysis of oxygen and sulfur isotope ratios in oxide and sulfide minerals by spot heating with a carbon dioxide laser in a fluorine atmosphere. *Accounts of Chemical Research* **27**, 237–241.

Salvi, S. & Williams-Jones, A. E. (1990). The role of hydrothermal processes in the granite-hosted Zr, Y, REE deposit at Strange Lake, Quebec/Labrador: evidence from fluid inclusions. *Geochimica et Cosmochimica Acta* **54**, 2403–2418.

Scaillet, B. & MacDonald, R. (2001). Phase relations of peralkaline silicic magmas and petrogenetic implications. *Journal of Petrology* **42**, 825–845.

Schmitt, A. K., Emmermann, R., Trumbull, R. B., Bühn, B. & Henjes-Kunst, F. (2000). Petrogenesis and $^{40}Ar/^{39}Ar$ geochronology of the Brandberg Complex, Namibia: evidence for a major mantle contribution in metaluminous and peralkaline granites. *Journal of Petrology* **41**, 1207–1239.

Sharp, Z. D. (1990). A laser-based microanalytical method for the in-situ determination of oxygen isotope ratios of silicates and oxides. *Geochimica et Cosmochimica Acta* **54**, 1353–1357.

Sheppard, S. M. F. (1986). Igneous rocks: III. Isotopic case studies of magmatism in Africa, Eurasia and oceanic island. In: Valley, J. W., Taylor, H. P., Jr & O'Neil, J. R. (eds) *Stable Isotopes. Mineralogical Society of America, Reviews in Mineralogy* **16**, 319–368.

Sood, M. K. & Edgar, A. D. (1970). Melting Relations of Undersaturated Alkaline Rocks. *Meddelelser om Grønland* **181**, 41 pp.

Späth, A., Le Roex, A. P. & Opiyo-Akech, N. (2001). Plume–lithosphere interaction and the origin of continental rift-related alkaline volcanism—the Chyulu hills volcanic province, Southern Kenya. *Journal of Petrology* **42**, 765–787.

Steiger, R. H. & Jäger, E. (1977). Subcommission on geochronology: conventions of the use of decay constants in geo- and cosmochronology. *Earth and Planetary Science Letters* **36**, 359–362.

Stephenson, D. (1972). Alkali clinopyroxenes from nepheline syenites of the South Qoroq Centre, South Greenland. *Lithos* **5**, 187–201.

Stephenson, D. (1974). Mn and Ca enriched olivines from nepheline syenites of the South Qoroq Centre, South Greenland. *Lithos* **7**, 35–41.

Stevenson, R., Upton, B. G. J. & Steenfelt, A. (1997). Crust–mantle interaction in the evolution of the Ilímaussaq Complex, South Greenland: Nd isotopic studies. *Lithos* **40**, 189–202.

Strong, D. F. & Taylor, R. P. (1984). Magmatic-subsolidus and oxidation trends in composition of amphiboles from silica-saturated peralkaline igneous rocks. *Tschermaks Mineralogische–Petrologische Mitteilungen* **32**, 211–222.

Taylor, H. P. J. & Sheppard, S. M. F. (1986). Igneous rocks: I. Processes of isotopic fractionation and isotope systematics. In: Valley, J. W., Taylor, H. P., Jr & O'Neil, J. R. (eds) *Stable Isotopes. Mineralogical Society of America, Reviews in Mineralogy* **16**, 227–269.

Upton, B. G. J. (1962). Geology of Tugtutôq and Neighbouring Islands, South Greenland. *I. Bulletin Grønlands Geologiske Undersøgelse* **34**, 60 pp.

Upton, B. G. J. & Emeleus, C. H. (1987). Mid-Proterozoic alkaline magmatism in southern Greenland: the Gardar province. In: Fitton, J. G. & Upton, B. G. J. (eds) *Alkaline Igneous Rocks. Geological Society, London, Special Publications* **30**, 449–471.

Upton, B. G. J., Stephenson, D. & Martin, A. R. (1985). The Tugtutôq older giant dyke complex: mineralogy and geochemistry of an alkali gabbro–augite-syenite–foyaite association in the Gardar Province of South Greenland. *Mineralogical Magazine* **49**, 624–642.

Valley, J. W. (1986). Stable isotope geochemistry of metamorphic rocks. In: Valley, J. W., Taylor, H. P., Jr & O'Neil, J. R. (eds)

Stable Isotopes. *Mineralogical Society of America, Reviews in Mineralogy* **16**, 445–486.

Valley J. W., Kitchen, N., Kohn, M. J., Niendorf, C. R. & Spicuzza, M. J. (1995). UWG-2, a garnet standard for oxygen isotope ratios: strategies for high precision and accuracy with laser heating. *Geochimica et Cosmochimica Acta* **59**, 5223–5231.

Vennemann, T. W. & Smith, H. S. (1990). The rate and temperature of reaction of ClF_3 with silicate minerals, and their relevance to oxygen isotope analysis. *Chemical Geology* **86**, 83–88.

Wones, D. R. (1989). Significance of the asssemblage titanite + magnetite + quartz in granitic rocks. *American Mineralogist* **74**, 744–749.

Zheng, Y.-F. (1993*a*). Calculation of oxygen isotope fractionation in anhydrous silicate minerals. *Geochimica et Cosmochimica Acta* **57**, 1079–1091.

Zheng, Y.-F. (1993*b*). Calculation of oxygen isotope fractionation in hydroxyl-bearing silicates. *Earth and Planetary Science Letters* **120**, 247–263.

APPENDIX: MINERAL ABBREVIATIONS USED IN FIGURES AND TEXT

Mineral	Abbreviation
Ab	albite
Aeg	aegirine
Aeg-aug	aegirine–augite
Aen	aenigmatite
Alkfsp	alkali feldspar
Alm	almandine
Am	amphibole
An	anorthite
Andr	(hydro)andradite
Ap	apatite
Arf	arfvedsonite
Astr	astrophyllite
Aug	augite
Cc	calcite
Di	diopside
En	enstatite
Fa	fayalite
Fe-Act	ferro-actinolite
Fl	fluorite
Fo	forsterite
Fs	ferrosilite
Gro	grossular
Hed	hedenbergite
Hem	haematite
Ilm	ilmenite
La	larnite
Mag	magnetite
Ol	olivine
Or	orthoclase
Py	pyrope
Qtz	quartz
Rhö	rhönite
Rhod	rhodochrosite
Sid	siderite
Sp	spessartine
Ti-mag	titanomagnetite
Tit	titanite
Usp	ulvöspinel
Wilk	wilkinsonite
Wo	wollastonite
Zrn	zircon